UNIVERSITY OF OKLAHOMA
GRADUATE COLLEGE

PALEOECOLOGY OF THE MORENO HILL FORMATION (TURONIAN-CONIACIAN, CRETACEOUS) OF NEW MEXICO

A THESIS

SUBMITTED TO THE GRADUATE FACULTY

in partial fulfillment of the requirements for the

Degree of

MASTER OF SCIENCE

By

IAN ALEXANDER TAYLOR
Norman, Oklahoma
2023

PALEOECOLOGY OF THE MORENO HILL FORMATION (TURONIAN-CONIACIAN, CRETACEOUS) OF NEW MEXICO

A THESIS APPROVED FOR
THE SCHOOL OF GEOSCIENCES

BY THE COMMITTEE CONSISTING OF

Dr. Richard Lupia, Chair

Dr. Shannon Dulin

Dr. Jacqueline Lungmus

ABSTRACT

The Cretaceous Terrestrial Revolution was a period of diversification of all major terrestrial groups that coincides with the rapid evolution and establishment of angiosperms (flowering plants) that began ~125 million years ago. The Moreno Hill Formation (MHF) was deposited over a two-million-year span of time during the late Early Cretaceous (90.9 Ma-88.6 Ma) and is a near-shore terrestrial deposit, except for a marine incursion near the base of the formation. The Moreno Hill Formation coincides with the first peak of angiosperm diversity in the Cretaceous. A moderately diverse vertebrate fauna has been recovered from the MHF including several members of Dinosauria. To better understand the ecology and climate of the formation, I analyzed four fossil wood specimens—three from the lower member and one from the upper member—to determine the taxonomic relationships of those woods, and the climate during deposition of the Moreno Hill Formation. On the basis of character analysis, all four specimens are assigned to *Cupressinoxylon* sp. aff. *C. manuelli*. The growth habits of the woods from the lower member and the wood from the upper member were found to be different suggesting a change in climate from the lower member to the upper member. I also developed a new method for the analysis of palynodebris (acid-resistant organic remains) using samples that were collected from the upper member of the Moreno Hill Formation. I utilized the Malvern Morphologi G3 morphometric microscope and its associated software. My new protocol to automate collection of palynodebris data was compared to data collected by conventional analysis in order to evaluate the method's efficacy. I then used both data sets to interpret changes in taphonomic signatures that could affect interpretation of paleoecological data from the Moreno Hill Formation.

Table of Contents

Chapter 1

INTRODUCTION

The Cretaceous Terrestrial Revolution began with the first major radiation of angiosperms (flowering plants). The diversification of this clade is then followed by increases in diversification of most terrestrial groups and the establishment of many ecological constituents that persist into the modern day. Fossil evidence suggests the first major radiation of angiosperms occurred during the middle of the Early Cretaceous between 110 and 100 million years ago (Benton et al., 2021). Factors both biotic and abiotic drove this rapid diversification in angiosperms. Mutualistic relationships began to form with pollinating insects which drove the diversification of both groups. Ferns also experienced a sharp increase in biodiversity as many members of the group became epiphytic (i.e., using another organism as a substrate). This is thought to be a direct result of the rapid diversification of angiosperms as the available substrate for epiphytes would have increased greatly as angiosperms diversified and radiated (Benton et al., 2021).

An increase in fungal diversity is also recorded at this time (Benton et al., 2021). This is due to the rapid life cycles angiosperms have, and their tendency to produce large amounts of litter throughout their life cycle. Angiosperms developed specific adaptations to transport water effectively (e.g., higher stomatal density, higher vein density, differentiation of tracheid cell types into fibers and vessels). These adaptations move water effectively and also permit the

individual to tolerate higher rates of evapotranspiration (Benton et al., 2021; Singh et al., 2021). These features led to angiosperms to produce more leaf litter. The newly abundant leaf litter led to increases in groups that use decaying organic matter as a nutrient source. Not only fungal diversity but also detritivore diversity increased likely as a direct result of an increase in the amount of leaf litter. In addition, the increase in insect diversity likely in turn drove the increases seen in many other groups. Arachnids experienced a large increase in diversity as did birds, squamates and mammals (Benton et al., 2021). Thus, the mutualistic relationships between angiosperms and insects not only caused both groups to radiate, but also resulted in greater amount of available food sources for other groups (Benton et al., 2021).

Environmental factors that drove, or at least facilitated, angiosperm diversification were equally numerous. Increasing carbon dioxide concentrations in the atmosphere, during the Early Cretaceous, itself the result of increased vulcanism driven by an increase in tectonic activity contributed to a warming climate. An increase in seafloor spreading during the Early Cretaceous led to increases in oceanic temperatures globally (Benton et al., 2021; Francis et al., 1993). Epeiric seas became common globally during the Early and 'middle' Cretaceous due to a lack of continental glaciers, generally young, therefore shallow global oceans, the opening of new basins due to tectonic activity and the thermal expansion of ocean water (Benton et al., 2021; Francis and Frakes, 1993). For example, in North America, the Sevier Orogeny resulted in the formation of the Western Interior Basin that would later hold the Western Interior Seaway. All of these factors contributed to the climatic conditions under which angiosperms first diversified and became significant drivers of ecologic interactions.

The Moreno Hill Formation represents over two million years of a depositional history that records the transition of the Turonian into the Coniacian (Cilliers, et al., 2021). There are

three distinct members of the Moreno Hill Formation with the lower and upper members representing two distinct terrestrial climates (Cilliers et al., 2021). Also, of interest within the Turonian-Coniacian transition are the vertebrate fauna found there. Tyrannosaurids, hadrosaurids, dromaeosaurs, therizinosaurs, and the ceratopsian taxon *Zuniceratops christopheri*, which is the oldest North American ceratopsian with brow horns and may represent a basal member of the clade Neoceratopsidae, have all been found within the Moreno Hill Formation and are some of the earliest representatives of clades that persist in North America through to the end of the Maastrichtian (Lucas et al., 2000; Wolfe et al., 1998). The abundant vertebrate record in this unit makes the data contained within the Moreno Hill Formation invaluable in the understanding the ecological relationships during this interval of the Cretaceous.

Geologic Setting—Zuni Basin and Moreno Hill Formation

The development of the Western Interior Seaway is genetically related to the sediments found in the Laramidian Zuni Basin and the presence of the fully connected seaway had direct effects on the depositional environment of the MHF (Cilliers et al., 2021; Kauffman, 1985). The tectonic regimes to the west and south during the Late Jurassic (Bathonian, Kimmeridgian, or Tithonian?) and into the Cretaceous are partially responsible for the marine transgressions and regressions that typify many of the sediments along the corridor known as the Western Interior Basin (Cilliers et al., 2021). There are two major types of tectonism that are responsible for the basin development that led to the oceanic encroachments both to the north of the Zuni Basin and to the south of that basin that eventually led to the full connection of the Western Interior Seaway during the Aptian-Albian stages of the Cretaceous. That fully connected seaway lasted

through the Coniacian and into the early Maastrichtian before uplift and slowing tectonism allowed the oceans to drain off the continent.

The geographic proximity of the Sevier/Cordilleran foreland basin to the north in Colorado and Wyoming and the southern rifting complex south of it, culminated in the connection of both basins into the much larger Western Interior Basin. The oceans in both the north and south underwent a few transgressional events, resulting in retrograding/prograding shoreline sequence cycles in both the southeastern portion of the Sevier/Cordilleran foreland basin, which is in Colorado today, and in the rifting basin complex to in the south in what is now New Mexico and Texas. Shoreline retrograding sequence are then overlain with shallow marine sediments before finally giving way to deep marine sediments in both basins (Haenggi, 2002; Kauffman, 1985; Yonkee and Weil, 2015). These facies represent the first prolonged connection of the seaway. The deepening and connection of those basins allowed the transgression of the ocean to fully connect the two separate epeiric seas into the Western Interior Seaway that dominated the depositional environment of the western United States for the most of what remained of the Cretaceous (Kauffman, 1985). The full connection of the Western Interior Seaway and the accretionary orogenic event to the west effected the depositional systems of the eastern shoreline of Laramidia throughout the remainder of the Cretaceous the Moreno Hill Formation represents such an environment.

The Moreno Hill Formation (MHF) is preserved in the structural Zuni Basin between the Zuni and Defiance uplifts and the Nutria monocline, which formed after deposition. The Moreno Hill Formation lays north of the Mogollon highland slopes and has been interpreted as a terrestrial deposit and defined as a clastic wedge with the thickness of the unit ranging from between 4.75-261.5 meters (Figure 1). The Moreno Hill Formation overlies the Atarque

Sandstone, a Turonian shoreface deposit, and is overlain by the Eocene Baca Formation or the Miocene Fence Lake Formation, which are locally variable (Cilliers et al., 2021).

At its contact with the Atarque Sandstone, there is evidence of a marine incursion at the base of the MHF, at which carbonaceous mudstones grade into siliciclastic mudstones followed by a coal seam in the first ten meters of the formation (Cilliers et al., 2021; Hoffman, 1994). For, the next thirty-five meters of the lower member, the sediments grade into more siliciclastic mudstones that are interbedded with carbonaceous mudstones, coal seams, and more channel sands as we move up towards the middle member of the MHF (Cilliers et al., 2021; Hoffman, 1994). These shifts in depositional environment during the sedimentation of the lower member are likely related to variations in base level rather than large eustatic fluctuations (Cilliers et al., 2021).

The middle member of the MHF is just over ten meters thick and is represented by sequences of channelized sandstones ranging from 1-3 meters in thickness that are interbedded with thin laminated mudstone sequences that measure less than one meter thick (Cilliers et al., 2021; Hoffman, 1994). These clastic facies likely represent further tectonic uplift of the entire basin, moving the base level of the area to a topography that would encourage the deposition of alluvial channel sands of a braided stream deposit (Cilliers et al., 2021; Hoffman, 1994). The mudstone lenses in between the channel sands are thought to represent the lateral fining sequences typical of crevasse splays of alluvial systems (Cilliers et al., 2021; Hoffman, 1994; Sweeney et al., 2009).

The upper member of the MHF, much like the lower member, is dominated by laminated mudstones interbedded with carbonaceous mudstones of varying thickness and two large sequences of channelized sands near the middle and top of the upper member (Cilliers et al.,

2021). Sequences of carbonaceous mudstone lie on top of the youngest channel sands which then grade into siliciclastic laminated muds that continue to the top of the formation. The uppermost beds of the MHF are unconformably overlain, locally, by either the Eocene Baca Formation or the Miocene Fence Lake Formation (Cilliers et al., 2021; Hoffman, 2021). The depositional systems of the upper member are likely the result of a regression of the Western Interior Seaway coincident with the Niobrara Cyclothem, which would have positioned the location of the preserved MHF section further from the shoreline during the deposition of the upper member. This is exemplified by the similar depositional facies found in the upper and lower members but by the fewer number of coal seams in the most upper member (Cilliers, et al., 2023).

The age of the MHF has recently been constrained with much greater accuracy by Cilliers et al. (2021). By using detrital zircon analysis from crystals sampled at three different stratigraphic positions within the MHF and one sample taken from the Dakota Sandstone (below the Atarque Sandstone), those researchers were able to refine the duration of deposition of the MHF to ~2.3 Ma (Cilliers et al., 2021). The age of the Atarque Sandstone, which directly contacts the lower MHF, had been constrained previously using biostratigraphic methods to be no older than 93.4 Ma with a second phase of sedimentation occurring no later than 92.5 Ma. The deposition of the MHF occurred in two distinct phases. Deposition of the MHF began around 90.9 (± 0.5) Ma, which sets the beginning of deposition in the latest part of the Turonian Age. The middle member of the MHF marks the onset of the second phase of deposition that began sometime after 88.6 Ma, which puts the second phase of sedimentation during the earliest Coniacian (Cilliers et al., 2021). These discontinuous sedimentation phases were the result of tectonic uplift to the west and south and likely influenced by the behavior of the Western Interior

Seaway, specifically the Greenhorn Formation and Niobrara Formation cyclothems that record transgressions and regressions of the seaway (Cilliers et al., 2021; Kauffman, 1985).

The focus of my investigation is to further elucidate the paleoecology and paleoclimate of the Moreno Hill Formation by analyzing four specimens of petrified wood found at different stratigraphic horizons within the MHF. Three of the specimens were collected from the lower member of the MHF. The fourth specimen was collected in the upper member of the MHF (Figure 2). In addition to the fossil wood, palynological samples stratigraphically associated with some of the vertebrate taxa found within the formation were also collected in the upper member of the MHF. I develop a new method for rapidly analyzing palynodebris—pollen, spores, wood fragments, cuticle, and other acid resistant remains—in order to identify isotaphonomic sample sets and depositional facies in which plant and dinosaurian constituents were recovered. The identification of this wood and the analysis of palynodebris helps elucidate some of the ecological and climatic constancy, or lack thereof, during the deposition of the Moreno Hill Formation and will grant greater insight into the environmental conditions over its more than two-million-year history of deposition.

Chapter 2

CUPRESSACEOUS WOOD FROM THE MORENO HILL FORMATION

Four fossil wood specimens were collected at multiple localities within the Moreno Hill Formation in the Eagle Peak Wilderness Study Area, Catron County, New Mexico. The Eagle Peak Wilderness Study Area is federal land administered by the Bureau of Land Management (BLM) Socorro District. All fieldwork and collections were performed under BLM collection permit (NM 21-04S) held by Dr. Richard Lupia, University of Oklahoma. All specimens are reposited in the Paleobotany, Micropaleontology and Mineralogy Collection of the Sam Noble Oklahoma Museum of Natural History, University of Oklahoma, Norman, Oklahoma. For convenience and clarity, individual wood specimens in this thesis are referred to by their Oklahoma Paleobotany Collection (OPC) number representing the sampled specimen and all its derivatives. Unique catalog numbers have been assigned to each derivative—e.g., blocks, fragments, billets, thin sections—and those derivatives are available for inspection by referencing the OPC number. Microscopic slides of radial, transverse and tangential sections of modern *Juniperus virginiana* L. (Plate IV) were provided by Dr. Abigail Moore, University of Oklahoma, for comparison.

OPC2462, OPC2464, and OPC2465 were collected within the lower member of the Moreno Hill Formation; the coordinates of these collection sites are: 34° 20’ 9” N, 108° 42’ 55” W; 34° 20’ 7” N, 108° 43’ 1” W; 34° 20’ 7’ N, 108° 43’ 00” respectively. OPC2462 was collected as float in a gully within five meters of the base of the section. OPC2464 was collected as float on the surface; its origin is unknown, but as found was stratigraphically between OPC2462 and OPC2465. OPC2465 was collected *in situ* in contact with a layer of gray mud

below OPC2464 and also within the first five meters of the MHF (Figure 3.) OPC2469 was recovered ~11 km from the collection areas of the first three specimens very close to the top of the section at coordinates 34° 23' 15" N 108° 37' 4" W, as float on a hill slope above a sequence of channel sands.

The specimens were prepared by using a brick saw and cutting the specimens into blocks that revealed well-preserved radial, transverse, and tangential sections. Those cut blocks were then sent to Wagner Petrographic (122 1800 W STE 7, Lindon, UT 84042; https://www.wagnerpetrographic.com) for the preparation of petrographic thin sections for microscopic analysis. A billet was made from each block by embedding in resin. An uncovered petrographic 2"x3" thin section was made from each billet following standard techniques.

Taxonomic determinations to the genus level were made using Bamford and Philippe (2001) and Philippe and Bamford (2008). Determinations to the species level were derived from comparisons with previous publications on fossil wood that described related taxa within Cupressaceae and *Cupressinoxylon* (Barber, 1898; Herrera et al., 2017; Lutz, 1930; McIver, 2001; Ríos-Santos et al., 2020). The type specimen of *Cupressinoxylon jurassica* Lutz 1930 was also analyzed for taxonomic comparison. Comparisons with modern taxa were performed using the IAWA Soft Wood identification schema (https://insidewood.lib.ncsu.edu/welcome, https://www.iawa-website.org/uploads/soft/Abstracts/01_IAWA-Softwood_List.pdf). Measurements are given in mean(minimum-maximum) notation.

The majority of features relevant for taxonomic determination are found in radial view. Cross-fields are the intersection of longitudinal tracheid and ray parenchyma cells. The number of pits per cross-field, which are structures used to conduct water, as well as the shape of the pit aperture of those cross-field pits are important to the taxonomic determination of fossil wood

genera (Philippe et al., 2008). The arrangement of longitudinal tracheid pits in radial view are also taxonomically relevant. These pits also function as zones of water transport between cells (Philippe et al., 2008). Axial parenchyma cells function as the cells that transport sugars to from zones of photosynthesis to other cells in the living wood. The shape of the end walls of those cells and their arrangement, zonate or diffuse in tangential view, provide more specific information taxonomically. Ray parenchyma, cells that move water towards the outer layers of the wood, may provide information about the type of climate in which an individual lived (Phillipe et al., 2008). The height of the rays (in number of cells) and their seriation habit of (uniseriate, biseriate, mixed) can be used as characters for taxonomic identification though these features are less taxonomically significant than the cross-field habits or bordered pit arrangement (Bamford et al., 2001).

Taxonomy

Order: Coniferales

Genus: ***Cupressinoxylon*** Göppert, 1850 nom. Cons. Prop.

Type species: ***Cupressinoxylon gothanii*** Kräusel in Jahrb (1920) typ. cons.

Cupressinoxylon sp. aff. ***C. manuelli*** Ríos-Santos, Cevallos-Ferriz and Pujana 2020

Location: Eagle Peak Wilderness Study Area, New Mexico

Stratigraphic horizon: Moreno Hill Formation (lower and upper members)

Age: Turonian-Coniacian (Cretaceous)

Repository: Sam Noble Oklahoma Museum of Natural History, University of Oklahoma, Norman, Oklahoma.

Thin Section Analysis

OPC2462 Radial section analysis: Cross-fields usually exhibit only one pit per cross-field, rarely two and never more. Cross-field pitting shows cupressoid apertures exclusively. Where a cross-field with two pits are observed, other nearby cross-fields also exhibit two pits per field in localized or zonate arrangements. No large variation in cross-field pit size is observed between the cross-fields that hold one pit and the cross-fields that hold two the cross-field pits. The diameter of the cross-field pits measures 22(14-28) µm. However, there is a slight change in size of cross-field pits from the transition of earlywood into latewood, with late wood cross-fields being smaller, though this change is very slight (between 2-5µm) (Plate I, Fig. 1).

Bordered pit arrangement is predominately uniseriate with abietinean arrangement. Bordered pits are rarely contiguous, but where present, adjacent tracheids frequently bear contiguous pitting (that is, in localized zones) (Plate I, Fig. 2). Biseriation is very rare, comprising less than 10% of observed bordered pits. Where biseriate, tracheid pitting sometimes

showing an araucarian bordered pit arrangement, however this feature is rare. The edges of the bordered pits exhibit two common morphologies. Bordered pits with a smooth border are the majority of bordered pit morphology present (>95%); pits with notched borders make up the remainder. The notched borders are rare but easily distinguishable from their smooth bordered counterparts (Plate I, Fig. 4). Pit apertures are generally circular but sometimes exhibit a cupressoid shape, with the orientation of the long axis of the aperture being variable between 45^{o} and 325^{o}. Bordered pits measure 20.8(14.4-27.3) µm in diameter with a height-to-width ratio of 1.05(0.71-1.73). Tracheid dimensions are 36(17-52) µm wide.

Axial parenchyma is abundant and diffuse with rare instances of the dark contents within the cells. Axial parenchyma end walls are rounded and smooth, while the horizontal walls can be pitted or notched. The notching/pitting of horizontal walls may be an artifact of preservation as dark contents are always present in association with pitted and notched horizontal cell walls. Spiral deformation ("checking") is present and common proximal to cross-fields in radial view (Plate I, Fig. 3).

OPC2464 Radial section analysis: Bordered pit arrangement is the same as in OPC2462 with similar ratios of abietinean to araucarian arrangement. The morphology of the bordered pits is also the same as OPC2462 with both smooth and notched borders present in a similar abundance. Bordered pit diameter measures 17.36(11-21.95) µm with a height-to-width ratio of 0.96(0.73-1.35). Pit aperture behavior is the same as OPC2462 (Plate I, Fig. 6). Tracheid dimensions are 40(18-58) µm wide, a similar ratio of bordered pit to tracheid width is seen in OPC2462. Cross-fields exhibit similar arrangements and behaviors as OPC2462 although the cross-field pits are smaller in diameter, measuring 16(9-20) µm (Plate I, Fig. 5). Axial parenchyma exhibits the same habit observed in OPC2462, although horizontal walls are more often pitted, but again

always in association with dark contents proximal to the pitting. Spiral checking is present and common around regions of visible cross-fields. (Plate I, Fig. 8).

OPC2465 Radial section analysis: Bordered pit arrangement and habit is the same as in OPC2462, with bordered pits measuring 17.29(14.53-21.95) μm. Notched borders are also present in similar abundances to OPC2462 (Plate I, Fig. 12). Tracheid width is 34(21-57) μm giving a similar ratio of bordered pit diameter to tracheid diameter. Cross-fields show nearly identical arrangements as in OPC2462 with cupressoid shaped pit apertures and generally one pit per cross-field that measures 20(15-27) μm in diameter (Plate I, Fig. 9). Axial parenchyma end walls are rounded and smooth with some pitting or notched morphology on the horizontal walls in association with dark contents near the cell walls. Spiral checking is more common in OPC2465 than in OPC2462 or OPC2464.

OPC2469 Radial section analysis: Bordered pit arrangement is the same as in OPC2462 although pits are more rarely contiguous. Bordered pits where contiguous still exhibit zonate behavior across multiple tracheids (Plate I, Fig. 13). The shape and aperture of bordered pits are also consistent with OPC2462 with a small percentage of notched borders present. The diameter of bordered pits measures 20.7(13.4-25.6) μm with tracheid width measured at 39(17-58) μm. Cross-fields pit apertures are cupressoid and are generally limited to one pit per cross-field though two pits per cross-field do occur and are generally localized as in OPC2462. Axial parenchyma cells have smooth end walls and horizontal cell walls. Horizontal cell walls rarely exhibit the pitting or notched habit that are found in OPC2462, OPC2464, and OPC2465, though dark contents are present within the axial parenchyma cells. Spiral checking is common in proximity to cross-fields as in OPC2462.

OPC2462 Tangential section analysis: In tangential section long axis compression due to preservation expresses itself in the cell walls of the ray tracheids being destroyed or deformed perpendicular to the axis of compression (Plate II, Fig. 1). The preservation affects the measurement of the height of all rays but will not influence the number of cells counted in any given ray. Rays are diffuse throughout and are numerous. Most rays are uniseriate (98.23%). The number of cells per ray is 18(1-78) with height of the rays being 389(28-1504) µm. Tracheid width in tangential view is 30(16-45) µm. Axial parenchyma is common and diffuse in tangential view (Plate II, Fig. 1). Parenchyma cell walls are smooth and the endwalls are slightly rounded. Bordered pits are found in tangential view although they are rare (Plate II, Fig.2).

OPC2464 Tangential section analysis: Rays are diffuse and numerous, being primarily uniseriate (95.1%). The number of cells per ray is 14(1-53) and they measure 293(31-943) µm. Tracheid dimensions in tangential view are 35(15-55) µm with intertracheid pits affecting the outline of the tracheid cell walls as in OPC2462. Axial parenchyma is common and diffuse in tangential view as in OPC2462. Cell walls of axial parenchyma are smooth and endwalls are rounded as in OPC2462. Bordered pits are rarely found in tangential view as in OPC2462 (Plate II, Figs. 3-4)
OPC2465 Tangential section analysis: As in OPC2462, rays are diffuse and numerous and primarily uniseriate (92.91%). The number of cells per ray are 15(2-52) and the ray height is 292(43-943) µm. Tangential tracheid dimensions are 30(18-55) µm wide. Intertracheid pitting is visible and affects the shape of the tracheid cell walls, giving them a notched shape as in OPC2462. Axial parenchyma is common and diffuse in tangential section with rounded end

walls and smooth transverse cell walls. Bordered pits are also rarely observed in tangential section as in OPC2462 and OPC2464 (Plate II, Figs. 5-6)

OPC2469 Tangential section analysis: Rays are diffuse and numerous and exhibit primarily uniseriate habit. Unlike the other specimens however, the percentage of uniseriate rays are much lower (60.7%). Though rarely truly biseriate, many rays exhibit a "mixed" habit, some portion of the rays (above 25%) being biseriate and have been defined as having a "mixed" seriation habit. The number of cells per ray on the longitudinal axis are 20(1-49) and the heights of the ray's measure 355(25-891) μm (Plate II, Fig. 7). Tracheid width in tangential sections measure 31(15-60) μm similar to OPC2462, OPC2464, and OPC2465. Intertracheid pitting is present and affects the shape of the cell wall as in OPC2462. Axial parenchyma is diffuse with rounded end walls and smooth transverse walls. As in OPC2462 tangential bordered pits are observed but their occurrence is rare (Plate II, Fig. 8).

OPC2462 Transverse section analysis: Tracheid cell walls vary in shape from slightly rounded to pentagonal to square. The number of tracheids between rays varies between one and five cells. Seasonal growth rings are abrupt and distinct with the transition from earlywood to latewood being gradual over around 8 to 10 cells. Latewood growth rings are made up of rows of between two and four cells, with the cell walls thickening significantly before the abrupt transition back to earlywood. Intraseasonal growth rings are present and exhibit a gradual reduction in size of tracheid cells before gradually transitioning back into larger tracheid growth. The difference between intraseasonal and seasonal growth rings is easily observed with the gradual transition of earlywood to latewood and back to earlywood being distinct from the habit of seasonal growth

rings which have an abrupt transition from latewood back to earlywood (Plate III, Fig. 1). Axial parenchyma is diffuse in transverse section and lacks any regions of zonation (Plate III, Fig. 6).

OPC2464 Transverse section analysis: Thin section inadvertently not prepared by Wagner Petrographic.

OPC2465 Transverse section analysis: As in OPC2462, tracheid cell walls have various common shapes. The number of tracheids between rays is between one and five cells. Seasonal growth rings are abrupt with the transition from earlywood to latewood being gradual. Latewood growth rings are between two and four cells thick with the cell walls of latewood tracheid thickening significantly. Interseasonal growth rings are not observed in this specimen. At several areas that exhibit some of the initial behavior of latewood growth, there is significant destruction of the area across the entire zone of the specimen. This preservation feature occurs three times in the specimen perhaps indicating that the early-latewood transition is a zone of weakness. As in OPC2462 axial parenchyma is diffuse and lacks any regions of zonation (Plate III, Figs. 2, 4).

OPC2469 Transverse section analysis: As in both OPC2462 and OPC2465 tracheid shape is variable with the general shape being pentagonal to rounded and sometimes square. The number of tracheids between rays is also consistent with OPC2462 being between one and five tracheid cells (Plate III, Fig. 3). Seasonal growth rings transition abruptly back to earlywood with the earlywood to latewood transition being gradual. Seasonal growth rings are between two and six cells thick with some thickening of latewood cell walls. No intraseasonal growth rings are

observed in this specimen. Axial parenchyma is diffuse throughout the specimen and has no areas of zonation (Plate III, Fig. 5)

Discussion

The features present in all specimens are consistent with assignment of all specimens to the genus *Cupressinoxylon*, following Bamford and Philippe (2008). Nearly all ray cells are uniseriate except for some local biseriation. Axial parenchyma is present but is not associated with ray cells. Ray cell walls are smooth and unpitted. Radial pits are not scalariform, though some bordered pit features could be consistent with taxodiaceous wood. However, the non-contiguity and mostly abietinean arrangement of the bordered pits is not consistent. The presence and commonality of radial pits with notched borders excludes these specimens from *Taxodioxylon*. The shape and size of the apertures in cross-field in radial view further support the exclusion of theses specimens from *Taxodioxylon* (Table 1). The apertures of cross-field pits are cupressoid in shape and their orientation angle varies between 25^{o} and 345^{o}, the number of pits per cross-field being mostly one though sometimes two. Philippe and Bamford (2008) stated that these features could be shared among three genera of fossil wood; *Widdringtonoxylon*, *Tetraclinoxylon*, and *Cupressinoxylon*, though many of the features that separate those genera could be affected by taphonomic processes. The combination of all these features—one to two cupressoid pits per cross-field, abietinean bordered pit arrangement, the presences of bordered pits with notched borders, predominantly uniseriate tracheid pitting, the presence of tracheid pits in tangential walls of the tracheids, diffuse axial parenchyma, rays that exhibit a predominantly

uniseriate habit, distinct growth ring boundaries with gradual earlywood to latewood transitions—suggest that the specimens belong to the genus *Cupressinoxylon* Goppert, 1850.

For a determination to the species level, comparisons were made to 24 species of *Cupressinoxylon* from North America. Eleven of the 24 species are from rocks that are Cenozoic in age, two are from Jurassic sediments, eleven are Cretaceous in age, and one is of indeterminate age (*C. pannonicum* Unger 1850). These species were chosen as comparisons for their geographic and temporal proximity to the specimens from the MHF. The two Jurassic species *C. diskoense* Walton 1927 and *C. jurassica* Lutz 1930 differ from OPC2462, OPC2463, OPC2465, and OPC2469 in that the cross-fields exhibit up to three pits rather than one to two that the woods from MHF have. In addition, the number of pits per cross field is higher on average than in the specimens, being on average two to three pits per cross-field instead of one and only sometimes two (Lutz, 1930; Ríos-Santos et al., 2020).

In the Cenozoic woods *C. arkansanum* Knowlton 1891, *C. calli* Knowlton 1889*,* and *C. lamerense* Read 1930 the cross-fields are either poorly described or not described at all. However other features exclude them from being the same species as the wood found in the MHF: presence of resin canals in *C. arkansanum*, more pits per cross-field in *C. calli*, and rare axial parenchyma in *C. lamarense* (Ríos-Santos et al., 2020). In *C. dawsoni* Penhallow 1903, and *C. wilcoxense* Barry 1922 and *C. dubium* Cramer 1868 there are more pits per cross-field. In *C. wilcoxense* distinct growth ring boundaries are also present and in *C. dubium* there is the common presence of multiseriate radial pitting. In *C. polyomattum* Cramer 1868 and in *C. pulchrum* Cramer 1868 there is an absence of axial parenchyma. In *C. taxodioides* Conwentz 1878 there are frequent biseriate rays.

Of the Cretaceous taxa analyzed none of the cross-field features were described in detail therefore differences beyond cross-field habits had to be used to exclude these taxa. In *C. cheyennense* Penhallow 1900, biseriate and multiseriate radial pitting are present. This feature is also shared with *C. elongatum* Knowlton 1888 and *C. mcgee* Knowlton 1889 (Knowlton, 1888; Ríos-Santos et al., 2020). The Cretaceous wood species that have gradual earlywood to latewood trasitions include *C. borealis* Penny 1947, *C. wardi* Knowlton 1889, and *C. comanchense* Penhallow 1900. The five other Cretaceous taxa share features in common with the wood from the MHF. However due to a lack of descriptions of cross-field features no affinity could be determined for *C. bibbinsi* Knowlton 1896, *C. columbianum* Knowlton 1889, *C. coloradensis* Knowlton 1917 *C. glasgowi* Knowlton 1888, *C. pulchellum* Knowlton 1889, and *C. vermejoense* Knowlton 1917 (Knowlton, 1888; Ríos-Santos et al., 2020).

One recently described Cretaceous species of *Cupressinoxylon* holds most of the features present in the Moreno Hill Formation samples. *Cupressinoxylon manuelli* Rios-Santos, Cevallos-Ferriz and Pujana 2020 has well described cross-fields, with one to two pits per cross-field, cupressoid cross-field pit apertures, predominantly abietinean radial pitting with rare pit contiguity, and notched outlines on radial pit borders. Axial parenchyma is diffuse in *C. manuelli* as is the MHF wood and transverse walls are smooth in both the *C. manuelli* and the MHF specimens, growth ring boundaries are distinct, but the earlywood-to-latewood transition is gradual (Table 1). The rays in tangential view are predominately uniseriate with some mixed seriation and very rare instances of biseriate rays. These features are consistent with the MHF wood except for OPC2469 which will be further discussed below. Although, rare tangential tracheid pitting is present in all MHF specimens, it is absent from *C. manuelli*. The ratio between bordered pit diameter and tracheid width are also very similar between the MHF specimens and

C. manuelli (Table 1). *C. manuelli* has been found in northern Mexico in the Sonora region, found in alluvial mudstones of Campanian through Maastrichtian age.

Given the similarities between *C. manuelli* and all specimens from the MHF, as well as the close geographic-temporal relationship, I conclude that the wood from the MHF has a close affinity to *Cupressinoxylon manuelli*. Although they are not the same species definitively, the preponderance of shared features suggests a very close taxonomic relationship between the MHF wood and *C. manuelli*. Tracheid pits in tangential view are absent in *C. manuelli* (Plate II. Figs. 2, 4, 6, 8), and while axial parenchyma is tangentially zonate in the MHF wood, that feature is not present in *C. manuelli*. Although the Moreno Hill Formation specimens share a large number of taxonomically significant features with *C. manuelli*, and thus demonstrate a close affinity, there are features present in the MHF specimens that exclude it from a specific assignment to *Cupressinoxylon manuelli*.

Support for confident assignment to a fossil taxon belonging to the family Cupressaceae may be found in the features these fossil specimens share with extant taxa in this family. A close relationship has also been determined between the fossil wood from the MHF and the modern cupressaceous taxon *Juniperus virginiana* L. using the InsideWood database compiled by North Carolina State University (https://insidewood.lib.ncsu.edu/search?0) and the IAWA softwood standard key (https://www.iawa-website.org/uploads/soft/Abstracts/01_IAWA-Softwood_List.pdf) for identifying and coding morphologic features (Table 2). *Taiwania cryptomerioides* Hyata 1906 was also found to have a close taxonomic relationship with the MHF wood according to the IAWA key. However, *T. cryptomerioides* was excluded from that close relationship due to a preponderance of features mostly found in basal taxodiaceaeous taxa, e.g., cross-fields variable in aperture shape and generally more pits per cross-field (Table 1).

Juniperus virginiana and the MHF wood both exhibit abietinean arrangement of tracheid pits in radial view (Plate IV, Figs. 2-3). The ratio between bordered pit diameter and tracheid width is also comparable (Table 1). Bordered pits with notched outlines are present, as well as the number of pits per cross-field and the general shape of the cross-field pit apertures are cupressoid (Plate IV, Fig. 1). Growth ring boundaries are distinct, and the transition from earlywood to latewood is gradual. In transverse section axial parenchyma is diffuse and lack any areas of zonation as in the MHF wood (Table 1). The depth of the latewood boundary is generally between two and six cells deep (Plate IV, Fig. 7). In tangential view tracheid pitting is rare but present in *J. virginiana* and in the fossil wood specimens from the MHF. However, unlike the MHF wood, ray tracheid height is much smaller, between five and fifteen cells per ray, and are exclusively uniseriate. This differs significantly from the wood found in the MHF. Overall, the fossil wood shares many observed features in *J. virginiana* (Table 1, Table 2).

Growth Series Analysis

Extended sequences of growth rings through each tracheidoxyl ("growth series") were compiled and manually aligned using Adobe Illustrator from images captured of petrographic thin section's transverse view. A growth series was constructed for all three specimens of which transverse section slides were present. OPC2462 and OPC2465 are from the lower member of the MHF and OPC2469 is from the upper member near the top of the section (Fig. 4). An analysis of each growth series was performed with the following parameters in mind; the number of cells and height in μm that make up earlywood to latewood transition, the distance in between any two growth ring boundaries in μm, the delineation of seasonal growth rings and intraseasonal growth rings, and any perceived cyclicity of either seasonal growth rings or

intraseasonal growth rings. Gradual tightening of tracheid lumen size with no measurable thickening of the tracheid walls is indicative of intraseasonal growth ring habit. This gradual tightening is then followed by a gradual rebound of tracheid lumen diameter. Descriptions and measurements of each series will be listed from the from the innermost wood to the outermost wood (from bottom to the top in images). Cyclicity will be determined by the observation of any repeating patterns of seasonal or interseasonal growth rings (i.e., the occurrence of two interseasonal rings between two seasonal ones where that pattern then repeats itself in the successive interim between one seasonal ring and the next one).

In OPC2462 only three rings comprise the available series. The first ring is an intraseasonal growth ring. The intraseasonal ring is between ten and twelve cells in height and measures between 250-275 µm. Laterally, the wood of this ring is significantly crushed, likely through preservation (Plate III, Fig. 1), this habit is observed multiple times in the series and may be associated with growth rings and some structural weakness associated with growth ring development. The next growth ring in the series is ~12,000 µm beyond the first and exhibits behaviors of an intraseasonal growth ring. The height of this ring in the number of cells is between four and six cells, this is a much shorter duration of slowed growth than the previous ring and only measures between 100-125 µm. The final ring found in the series occurs less than 100µm from the previous ring. This final ring exhibits the behavior of a true seasonal growth ring. The ring itself is between four and six cells deep with the lumen of the tracheid cells shrinking as well as the tracheid cell walls thickening significantly. There is no gradual rebound of tracheid cell size, the boundary between latewood growth and earlywood growth is distinct and abrupt. The height of the ring is only between 75-100 µm. This seasonal growth ring is also associated with significant cracking and crushing of the specimen.

The growth series for OPC2465, which was the wood found *in situ*, produced a growth series with six seasonal and three intraseasonal growth rings. The first of these rings exhibits characteristics of seasonal growth rings with the transition from latewood to earlywood being abrupt. Due to preservational limitations, the number of cells that make up this transition cannot be determined but its height is around 120 μm. The next growth ring is 2000 μm from the first and exhibits the behaviors of an intraseasonal growth ring, the cycle of gradual tightening and expansion of the tracheid lumen occurs over twelve to fourteen cells and is 225 μm in height. This ring is associated with a small crack due to preservation (Fig. 4). The next ring in the series is found 6200 μm from the previous and is a seasonal one, with the number of cells within the ring being between 6-10, the number cannot be determined with more accuracy due to preservation. The height in μm is also indeterminate because of this preservation. Around 3000 μm from that growth ring, another seasonal growth ring is found in the series. This seasonal growth ring is between six and eight cells and is 110 μm in height. The transition from latewood to earlywood is distinct and abrupt. 7000 μm beyond that is another seasonal growth ring. The transitional period of this ring is longer than the previous seasonal rings, being between ten and twelve cells, with the height being 150 μm. The next ring in the series is an intraseasonal one found 4700 μm from the previous ring. The gradual tightening and expansion of the tracheid lumen occurs over six to eight cells which has height of 85 μm. The next ring in the series is found only 250 μm from this ring and also exhibits the behaviors of an intraseasonal growth ring. The transition duration of this ring is also between six and eight cells and measures around 100 μm. 1200 μm beyond that is another seasonal growth ring. The number of cells in this ring are between six and eight with a height of 110 μm. Less than 300 μm beyond that is the final ring of the series which exhibits behaviors of seasonal growth rings. The transition from latewood to

earlywood is distinct and abrupt and occurs over six to eight cells with a height of 120 μm. Even though there are several growth rings found in OPC2465, no cyclicity could be determined for either the seasonal or intraseasonal growth rings present.

The final growth series analyzed was that of OPC2469 which is from the top of the upper member of the MHF. The preservation of this sample is poor, with very little dark contents left within the cells which made the identification of certain features difficult. Despite the poor preservation rings were found within the series, the first being very near the base of the growth series. This first ring exhibits the behaviors of a seasonal growth ring with the transition from latewood to early wood being abrupt and distinct, with the lumens of the tracheid cells becoming smaller while the tracheid cell walls thicken across this transition. The transition occurs between 5 and eight cells with a height of 120 μm. The next ring in the series occurs 8500 μm from the first and exhibits the behaviors of a seasonal growth ring. This transition occurs over four to six cells and has a height of 100 μm. The final ring found in the series is found 1000 μm pat the second ring in the series and exhibits the behaviors of a seasonal growth ring. Across a transitional period of four to six cells lumen diameter shrinks while tracheid cell walls thicken up to the abrupt transition from latewood growth back into earlywood growth. This transition has a height of 110 μm. While there are only three growth rings present in the growth series for OPC2469, there does appear to be some cyclicity to the duration of a growth season within the sample. The growth rings are relatively evenly spaced and the difference in distance between all three of the seasonal growth rings is less than 200 μm.

The presence of only one seasonal growth ring and two intraseasonal growth rings which were associated with significant preservational destruction of the growth ring zones. Though the destructions of those zones make any determination of cyclicity difficult, the presence of two

interseasonal growth rings suggest that the individual experienced variability in the climate in which it lived. Given the environment of deposition these perturbations are likely the result of an increase in temperature causing water stress to the organism which would have experienced increased evapotranspiration rates as temperature increased. In OPC2465 however, the preservation was good and six seasonal growth rings were found and measured as well as three intraseasonal rings. While there is no cyclicity determined in the growth series for OPC2465 this growth series does hold interesting information about climatic stresses that the individual underwent during at least some of its lifespan. The lack of cyclicity found in the seasonal growth rings would suggest a highly variable (from season to season and between seasons) water and/or temperature regime. Given that in the lower member of the MHF the environment has been interpreted as a prodeltaic nearshore environment (Cilliers et al., 2021), it seems unlikely that water paucity is a driving factor in the variability of seasonal growth duration. However, an overabundance of water could also affect the growth of cupressaceous wood such as OPC2465. In a system such as the Moreno Hill Formation it would be possible for some areas to not be well-drained, which is evidenced by the coal seams found in abundance in the lower member. Of particular interest within the growth series for OPC2465 are the final two intraseasonal growth rings and the final two seasonal growth rings. That there are two intraseasonal growth rings less than 200 μm from each other which are then less than 300 μm from two true growth rings which are themselves less than 200 μm apart suggest that at least in this point in the individuals' development something rather drastic was occurring climatically. Geologic evidence points away from a lack of water, so it is likely that these rings either represent a prolonged period of an overabundance of water or some kind temperature fluctuation. Again geologic evidence suggests that the MHF represents a depositional environment that occurs during a significant period of

warming in the Cretaceous (Cilliers et al., 2021; Francis and Frakes, 1993). This growth series could represent an anomalous period of warming within the environment that the lower member of the MHF represents. Higher temperature can cause many plants to exhibit behaviors of water stress even when water is plentiful. If evapotranspiration rates increase enough due to a warming temperatures then an individual's growth habit may reflect the growth of an individual experiencing drought (Petersen and Hill, 1985; Singh et al., 2021).

The three seasonal growth rings that were found within the growth series from OPC2469 all exhibit a much more uniform duration of latewood growth compared to OPC2465. The space in between the rings is also much more regular, with a difference of less than 300 μm between the duration of growth season. This much more conservative growth could suggest a much more limited supply of water during the growth season. Given that there are no intraseasonal growth rings found, this individual experienced at least two growth seasons in a relatively stable climate. The upper member of the Moreno Hill Formation where this specimen was collected has been interpreted as being deposited during a regression of the Western Interior Seaway. The environment of the area would have become drier as the coastline moved farther away from the depositional system. This interpretation matches the geologic evidence of the mudstones in the upper member having evidence of pedogenesis (Cilliers, et al. 2023). These paleosols are likely fossil vertisols or gleysols as the beige and gray mudstones typically exhibit some minor features associated with pedogenesis (e.g., root traces, small pedons, conchoidal fracturing and slickensides; R. Lupia, field notes, 2021), and would have been moderately to poorly-drained moist soils (Lawson, 1990, Cilliers, et al. 2023).

Given the geologic evidence of a warmer drier climate, and the conservative growth habit that is found in OPC2469 this may explain the trend towards more biseriate rays that were found

in the tangential section of OPC2469. The ray cells of conifer wood are structures used in the transportation of water toward the outer portions of the tree (Riddle, 2011). If water supply became more limited in the upper member of the MHF as geologic evidence suggests, an increase in the seriation of ray cells could have improved water transportation an increased the efficiency of water transportation. The fact that OPC2469 has morphological features and growth habit of an individual with a consistent water supply supports the supposition that the upper member of the MHF was drier than the lower member due to the regression of the Western Interior Seaway that was occurring during the second phase of deposition found within the MHF.

Given that many of these features have traditionally been thought to be influenced by both climate and phylogenetic relationships, I can make the supposition that the climate tolerance of both the MHF wood and *Juniperus virginiana* are similar (Little, 2006; Page, 1990). *Juniperus virginiana* is a ubiquitous constituent of forests in eastern North America. It can be found in every state east of the 100th meridian and in Washington state in the northwestern United States as an "invasive" species of those forests (Lawson, 1990; Riddle, 2011). Its range extends north into Canada and Greenland and as far south as the Gulf of Mexico. The average annual temperature at the northernmost limits of its range is 4^{o} C and 20^{o} C at the southernmost limits of its range. The minimum average temperatures within the *J. virginiana* range are -43^{o} C in the north -7^{o} C in the south with maximum temperatures ranging from 32^{o} C in the northern regions to 42^{o} C in the southern limits of its range (Lawson, 1990; Riddle, 2011). *J. virginiana* has a very broad range of water tolerance in addition to its broad temperature tolerance. The lower limits of the annual precipitation within that range is 38 cm at the northwestern limits of its range to 152 cm in the southeastern range (Lawson, 1990; Riddle, 2011).

The types of soil regimes that *J. virginiana* can thrive in are also broad. The soils that are most common within its range are mollisols and ultisols, as well as vertisols and gleysols at the extrema of their range, though as with many other species, they tend to grow best in deep moist well-drained alluvial soils. Where growth conditions are most favorable *J. virginiana* generally does not become a dominant constituent of the ecosystem due to the competition with rapidly growing hardwood (angiosperm) species (Lawson, 1990; Riddle, 2011). *Juniperus virginiana* also grows well in deep well-drained upland soils as well as in shallow rocky soil with a thin solum (up to 20 cm) (Riddle, 2011). In addition to its high tolerance for a broad range of soil textures and depths, *J. virginiana* also has a very broad pH tolerance within its range (Lawson, 1990; Riddle, 2011). Soil pH ranges from 4.7 to 7.8 in habitats where *J. virginiana* is found, though it should be noted that the high calcium content within the leaves (needles) of *J. virginiana* does tend to affect the soil pH around the plant, increasing soil alkalinity over time (Lawson, 1990; Riddle, 2011). Although its leaf litter has a propensity to drive soil alkalinity up, *J. virginiana* is not especially tolerant of soils that are heavily alkaline; it tends to prefer more acidic soils with most favorable growth found in soils with a pH from 5.4 to 6.5 (Lawson, 1990; Riddle, 2011).

Given the similarities of features found in the MHF specimens and the modern taxon *Juniperus virginiana,* it is reasonable to infer that the climatic and ecological tolerance of both species are similar. That the Moreno Hill Formation itself likely represents a nearshore alluvial flood plain with high amounts of clastic input that was sometimes well-drained (i.e., the presence of fossil gleysols) and sometimes not well drained (i.e., the coal lenses that are common throughout the lower member) it would be reasonable to conclude that the environment that the MHF represents would have been an environment in which the modern taxa *Juniperus*

virginiana could have lived, and therefore likely supports the notion that the MHF specimens were a major constituent within the flora at the time. The climate during deposition of the MHF and the specific tolerance of the MHF wood specimens to that climate will be discussed below in the following section.

Discussion

The lower member of the Moreno Hill Formation would have been an ever-wet floodplain environment likely only a few kilometers from the shore of the Western Interior Seaway (Kelley, 1987). A system of streams and rivers braided across a low-lying basin with local topographic lows that would have been filled with water and contained large amounts of flora adapted to swampy poorly drained histosols. On the local topographic highs in this environment is likely where individuals of *Cupressinoxylon* aff. *C. manuelli* would be found, growing in the relatively more well drained vertisols and gleysols that are adjacent to the low-lying swampy areas. The variability of growth rate observed in OPC2465 suggests an inconsistent amount of water in the system, given the geologic evidence, coal seams, laminated mudstones etc., it is unlikely that a paucity of water resulted in the variability of growth rate in OPC2465. Rather, it is more likely that the individual was experiencing a high variance of water availability which resulted in inconsistent rates of seasonal growth and could account for the presence of intraseasonal growth rings.

The upper member of the MHF would have had a slightly dissimilar environment. As the Western Interior Seaway retreated, the region represented by the MHF became drier. The

occurrence of standing water encouraging the deposition of coals lessened as the seaway continued to retreat. While the area remained a floodplain, its elevation in relation to sea-level increased. This changed the energy within the system slightly, likely increasing the amount of energy feeding into the system from the streams that braided across it. Because of this high relative elevation, the soils became more well drained exhibiting pedogenic features common in vertisols and gleysols. While in the lower member those paleosols likely represented local topographic highs in the upper member those paleosols become more common and widespread suggesting the entire environment sat at a relatively higher paleoelevation than the lower member.

This change in water regime and climate is reflected in the morphological features of OPC2469. The conservative and steady rate of growth, along with the consistency of the height of the latewood transition suggest this individual experienced a much less volatile environment than the specimens found in the lower member. The other evidence that points to the upper member being more arid than the lower member is the increase in ray seriation in OPC2469. While still predominantly uniseriate, the percentage of rays with mixed seriation habit has increased by more than 25% in OPC2469. The ray cells in wood function as a transportation system for water, from the inside of the living wood towards the outside. If annual precipitation became scarcer it stands to reason that during the wetter periods within a season that the individual would be best served by moving as much water as possible into the outer portions of the wood. An increase in the seriation of rays would serve that function, as well as taking advantage of any water available during the drier periods of growth. While this seriation habit is not observed in *J. virginiana* within the end members of its modern climate regime, it could be concluded that those changes within that modern taxa are unobservable given the timescales of

morphological changes due to selective pressures. However, the wood in the MHF (OPC2469) could represent morphological variation due to the selective pressures of a changing climate. Even if that is not the case the wood from the MHF grants insight into the growth habits of these coniferous constituents across two distinct climatic regimes. The growth and morphological features present in both the specimens from the lower member and the one specimen from the upper member ratify the interpretations of the MHF environment made most recently by Cilliers et al. (2023). The lower member was far wetter and more proximal to the coast of the Western Interior Seaway than the upper member. That both the lower and upper member are two distinct phases of sedimentation is also supported by the difference in morphological features suggesting a drier climate present in the upper member, which is suggestive of a different water regime than the lower member experienced and therefore likely a change in the energy of the system.

All four of the tracheidoxyls analyzed from the MHF have a very close taxonomic relationship to each other. Although they occur in two separate sections that represent two distinct sedimentation intervals, up to 2 million years apart, the consistent presence on the landscape suggest two similar ecosystems were present. The older samples from the lower member of MHF was more ever wet and proximal to the shoreline of the Western Interior Seaway (Kelley, 1987). The second ecosystem, represented by the upper member of the MHF, was relatively drier although with a more stable water regime. The specimens from the MHF represent arboreal constituents of two distinct ecosystems over two million years of deposition. The morphological features present within these members of Coniferales reflect the physical response that these individuals had to the climate in which they grew.

The three specimens from the lower section all exhibit morphological features consistent with modern cupressaceous wood that live in similar environments as what the MHF is thought

to represent. In the lower member the presence of coal seams interbedded with mudstones that have some evidence of pedogenesis, suggests a constant supply of water and soils that were only sometimes well-drained. The presence of coals in the lower member point to a proximity to the shoreline, and the presence of standing water for long durations of time. While *J. virginiana* does tolerate the moisture regimes and pH conditions that are commonly associated with environments that could produce coal seams, they do not prefer it (Riddle, 2011). The specimen OPC2465 has a growth series that suggests a wide variability in growth rate and it is reasonable to conclude that the specimens found in the lower member of the MHF were likely most found further away from the standing water that produced the coal seams within the MHF. In the modern taxon *J. virginiana* specimens are rarely found within two miles of the coastline, and while rare in swampy habitats, they do live on the upland margins of swampland in the more well-drained soils surrounding swamps (Riddle, 2011). If the climatic tolerances of the MHF specimens are similar to *J. virginiana* then it is likely that those individuals lived in similar environments to those in which *J. virginiana* lives today.

The very slight differences in OPC2469 compared to the specimens from the lower member are likely the influence of different water regimes and a warmer climate. The upper member of the MHF does have coal seams, but at a much lower frequency and are much thinner units. That those coal seams are more common in the lower portion of the upper member and then are completely gone from the very top of the section is consistent with the interpretation that the upper member of the MHF was deposited during a regressional phase of the Western Interior Seaway (Cilliers, et al. 2023). That interpretation is also consistent with the growth habit of OPC2469 and the slight differences in the seriation index of OPC2469 as compared to the three specimens from the lower member. OPC2469 grew at a more conservative and steadier rate with

no intraseasonal growth rings observed in the growth series. This suggests a consistent water regime that the individual experienced during the duration of growth represented by the growth series. The increase in ray seriation could be a function of living in a drier well-drained soil. This interpretation of the presence of those morphological features would be consistent with a cooler drier climate, which would have been the case as the epeiric sea began to fall away from the continent during the second phase of deposition in the MHF. The presence of the same taxon both at the bottom of the lower member and at the top of the upper member also suggests that this species was a common constituent of the arboreal flora throughout the deposition of the Moreno Hill Formation.

While there has been an a palynological analysis of the (primarily lower) MHF conducted by Kelley (1987), further research into the floral constituency of the MHF has been limited. There have only been two descriptions of angiosperm wood from the MHF and the above analysis is the first description of gymnosperm wood from the formation. So, more information needs to be collected about the paleoecology of the area. That the sedimentation occurred during one of the proposed warmest eras of the Cretaceous and that it records a terrestrial environment whose water regime was directly affected by the regression of the Western Interior Seaway elucidates the paleontological importance of the MHF. Many of the dinosaurian constituents found in the MHF also represent some of the earliest members of the groups that would come to dominate the North American ecosystems of the Campanian and Maastrichtian that are the final chapters of the Mesozoic Era. By better understanding the overall ecology of the MHF we may be able to better understand the success of those groups that persisted through the remainder of the Cretaceous.

Chapter 3

A NEW METHOD FOR THE ANALYSIS OF PALYNODEBRIS

Palynodebris analysis is tedious and time-consuming work. The analysis of a single slide can take several hours and alone, yields minimal amounts of data. Only when numerous slides

are analyzed will patterns emerge and interpretation of palynofacies changes become possible. Palynofacies are roughly defined as the organic matter that is recovered from rock or unconsolidated sediment using the standard techniques for recovering palynological debris, the process of which is the digesting of a sample in hydrochloric and hydrofluoric acids (Batten and Stead, 2005). All rocks containing organic matter must have an associated palynofacies (Batten and Stead, 2005). There is no unified system of classification of constituents within a palynofacies. The size and shape of that material provides can provide information on the energy present in a depositional system while the classes of palynodebris can provide ecological context, such as climatic shifts and floral transitions (Batten and Stead, 2005).

According to Boulter (1994), Combaz (1964) identified three major types of palynofacies: palynomorphs, palynodebris, and amorphous organic matter. Subsequent authors delineated these groups further. Boulter (1994), Tyson (1995), and Batten (1996) all produced different classification systems of palynofacies. Boulter delineated palynofacies types into five types: palynomorphs, palynowafers, amorphous organic material, other palynodebris, and other. Palynomorphs are defined by Boulter as being spores or pollen or dinocysts, palynowafers are defined as cuticle well preserved wood and degraded woody material. Amorphous organic matter was defined by Boulter to be specks with no structured outline pale to brown in color without any identifiable structures present. Other palynodebris was defined as debris with structured outlines but no other discernable features with fungal hyphae and algal debris also falling in this category. Boulter defined the “Others” category as foraminiferal linings, particulate matter that had some curvature was pale in color and had no openings (Boulter, 1994). Tyson categorized palynofacies in two main categories, structured and unstructured. Structured classes consist of palynomorphs that is then subdivided into zoomorphs, which are foraminiferal remains,

phytoplankton, defined as algal constituents and dinocysts, and sporomorphs, which are spores and pollen. Also, within the structured class are phytoclasts that include wood, cuticle and fungal hyphae. Tyson's unstructured class consists of amorphous organic material (Tyson, 1993). Batten defined three main palynofacies types: palynomorphs, structured organic matter, and unstructured organic matter. Palynomorphs are subdivided into spores and pollen, fungal reproductive material, dinocysts, acritarchs, algal constituents, and foraminifer linings. Structured organic matter includes phytoclasts such as wood (both brown and black), coalified matter, cuticle, tubes and filaments, and fungal hyphae. Unstructured organic matter was split into two subclasses: amorphous organic matter of aqueous origin and amorphous organic matter of terrestrial origin (Weller, 2004; Batten and Stead, 2005). Although these classification schemas are subjective, they share commonalities in their definitions of classes. The underlying unifier in all schemas is the analysis of different morphological parameters that any one constituent within a palynodebris slide might have. Color, elongation, circularity, perimeter, size, and translucence are all components that are considered when classifying different types of palynodebris, so while there is no standard classification of palynofacies, the types of measurements that define any class of palynofacies can in principle be objectively measured.

Palynodebris analysis has several applications. Because of the large number of organismal remains that can be found in palynodebris, those constituents may be useful in biostratigraphy. Planktonic organisms and pollen and spores tend to be widespread, and their remains tend to be highly resistant to decay and taphonomic processes. This allows those constituents to be useful markers of time in stratigraphic analyses. Palynofacies also represent very short amounts of sedimentological time which improves accuracy when dating a particular stratum according to the biologic constituents present (Weller, 2004; Batten and Stead, 2005;

Boulter, 1994). Palynodebris is also important in the interpretation of ecosystems and environments. Any pollen or spores present may indicate (subject to taphonomic processes) the biota present at or before the time of deposition. That biota can also be used to indicate the climate at the time of deposition. Plant debris and its distribution within palynofacies can provide information on the transport behavior of a sedimentary system based on size shape and type. These distributions provide information about the type and amount of transport the palynodebris has undergone and help assess how much degradation the organics of the system have undergone since burial. Tyson and Follows (2000) found a correlation between the quantitative values of size, shape, and abundance and the distance of transportation from the source (Weller, 2004; Tyson, 1993).

Significant differences in palynofacies between two different lithologies are expected. For example, the palynofacies found within a laminated mudstone should be different than a palynofacies found in channel sands simply because those two systems vary markedly in the energy of fluid flow at the point of deposition. Equally important, when trying to understand ecological shifts in an environment, is identifying the presence of any shifts in recovered palynofacies within a single depositional system. These shifts could represent floral assemblage transitions or simply track very variations in the energy of a depositional system, or both (Batten and Stead, 2005). Therefore, an assessment—qualitative or quantitative— of the palynodebris, beyond just examination of fossil organismal remains (e.g., pollen, spores, dinoflagellates, etc.) is critical.

The large time investment necessary for this type of analysis is what led me to look into alternative avenues for analyzing palynodebris. A single person may take several hours of palynodebris analysis just to produce a few hundred data points for one slide. Is there some sort

of automated system that would allow the user to gather large amounts of data from numerous slides/samples quickly, to make any shifts in palynofacies apparent to the user?

In 2004, Weller presented a system for the semiautomated classification of palynodebris. Using an automated microscope stage and by implementing an assisted neural network program, he developed a technique to identify different palynodebris types unassisted (by a human operator) based on images captured by a camera attached to the microscope upon which the automatic stage was set. This system of classification was found to be incredibly accurate in identifying and classifying palynodebris; his use of high-resolution image analysis yield confidence intervals of identification at 87%. After two more subsequent publications on this method. Weller did not publish on his methodology again. Weller et al., (2007) noted an increase in accuracy of two supervised neural networks that increased the classification confidence from 87% to 91%. While this technique is very useful for the classification of palynomorphs and other palynodebris types it relies on the compilation of many input images to "train" the neural networks.

So now my question became: do the data collected need to be at the level of resolution that Weller's method produces to still get accurate information about palynofacies present within a single depositional system? In other words, is there a faster, off-the-shelf tool that can be used to gather the same types of measurements collected by Weller's method, but without the employing a classification schema that would necessitate the development of some kind of machine learning neural network to resolve categorizations?

The sedimentology lab run by Drs. Lynn and Michael Soreghan, University of Oklahoma, has an automated morphological microscope housed within it. The Malvern Morphologi G3 (MG3) morphological microscope was developed and produced by Malvern

Panalytical and is conventionally used by pharmaceutical companies to analyze dispersion, breakdown etc. of pharmaceuticals. In the Soreghan lab, the MG3 is used to better understand sedimentological transport, grain size distributions, chemical composition, etc. of unconsolidated sediment, either in prepared slides or by sample dispersion. The MG3 has an automated stage and measures particles in the range from 2.5μm to 250μm under the 10x magnification setting. It measures these particles by taking pictures of each particle within a given sample, and then using the pixels in each image of that particle to take morphologic measurements.

For my purpose, the MG3 provides an opportunity to collect morphologic data on palynodebris slides that are 1) rapidly gathered, 2) of high sample sizes, and 3) potentially not biased by the observer or a subjective classification scheme. Not only does it take the measurements, but it also processes the information quickly and its associated software produce graphs for each morphologic parameter measured, making comparisons between samples incredibly efficient. As stated above it can take several hours of palynodebris analysis by hand to produce a statistically significant number of data points, while the MG3 can run a transect of an entire slide in around twenty minutes. In that twenty minutes the number of particles measured can reach into the hundreds of thousands, with at least six significant (to palynofacies analysis) morphological characteristics measured for each particle. The ability to gather and parse that much information in such a short amount of time can significantly change the rate at which palynofacies are interpreted. With the quick turnaround on data collection much more complete palynofacies analyses can be completed quickly, turning what would have been weeks or months of work into only a few hours of data collection.

Methods and Materials

The Malvern MG3 morphological microscope and its associated software (v.8.11), released in September of 2007 by Malvern Panalytical, is an automated microscope with an automatic stage that captures images of particles within a sample. Those images are then used for various morphometric measurements, e.g., Area in μm^2, Circularity, Convexity, Aspect ratio, etc. Once those measurements are collected the associated software allows the user to compare different variables within a sample and produces various graphs and charts for the user. Of particular interest when analyzing palynodebris are the dendrograms (from a cluster analysis, although the algorithm and similarity metric are not specified) that the software produces for several important morphologic variables. Those relationships can then be analyzed between slides to determine any potential underlying taphonomic changes that occur within a depositional system. This application of the Malvern MG3 to palynodebris analysis is novel, and a complete methodology had to be developed and tested first.

The organic matter from the processed samples was mounted on slides by Global Geolab, Ltd. (Alberta, Canada) without sieving (a.k.a. kerogen slide) and then were sieved first using a 5µm aperture mesh and slides prepared, them sieved with a 10µm aperture mesh and slides prepared. Due to low yield, sample OPC2455 only yielded a kerogen slide and one 5µm slide. All other samples were productive enough to produce kerogen, 5µm and 10µm slides. Kerogen slides were not analyzed due to the low level of particle dispersion found in kerogen slides and the moderate particle dispersion that the MG3 requires for accurate analysis.

To ensure the accuracy of the data collected from the Malvern, seven palynodebris slides from the MHF were used to ratify the data collection by the MG3. Slides from OPC2442, OPC2453, OPC2456, OPC2458, OPC2459, OPC2460 and OPC2461 were used and chosen for the observed variability of palynodebris content to test the accuracy of the MG3. Within the

software a “standard operating procedure (SOP)” was created to analyze the slides. The SOP was set up to analyze a transect of each slide by drawing three separate squares onto the slide analysis area within the software (Fig. 5). A transect of a single slide can be automatically analyzed in less than twenty minutes. The sample carrier on the MG3 holds four slides, and a single SOP is used to analyze all slides, meaning four slides can be analyzed in around an hour and a half. Because palynodebris is generally less than 500 µm, and because an object that fills more than 30% of the field of view will not be measured, the magnification of the SOP was set at 10x. To test the accuracy of the counts and measurements each slide was run under three different color and lighting parameters.

1. first run was done under the standard lighting Intensity of 80.00 and the standard greyscale mode.
2. second was performed at a lower light Intensity of 75.00 and used the software’s color mode.
3. third run for each sample is under 70.00 light Intensity in color mode and then used the software’s “white balance” mode (Fig. 6).

The six MG3 variable selected for analyses were: Area (µm^2), Circularity, Convexity, Aspect ratio, Solidity, and Intensity SD (standard deviation).

1. Area (µm^2) is the length times the width of a particle (Particle Characterization Guide, 2015). Area (µm^2) has no analogue in conventional palynodebris analysis but is a measure of particle size. Area (µm^2) has implications for the energy regimes within a system and are an important parameter in the separation of different palynodebris classes.
2. Aspect Ratio is the ratio of major to minor axes and is measured from 1 (circle/square) to infinity (infinitely elongate). The MG3 inverts this and measures from 0 (elongate) to 1

(circle/square). Elongate particles provide information distance traveled before deposition. It is a character of structured organic material (Particle Characterization Guide, 2015).

3. Circularity is the actual perimeter of a particle divided by the perimeter of a circle with equivalent Area (Particle Characterization Guide, 2015). Circularity can be construed as a measure of the abundance of pollen and spores (although monolete, monosulcate, and monocolpate tend oval) compared to other debris. Circularity partially overlaps with conventional 'equant' debris, i.e., those particles that show a ratio of major to minor axes near one but differs in being sensitive to angular particles. Amorphous debris is typically strongly circular. Circularity varies between 0 and 1.
4. Convexity is the convex hull perimeter of a particle divided by the actual perimeter of the particle. The convex hull perimeter is the perimeter of the entire field of a particle (Particle Characterization Guide, 2015). Convexity is a measure of how convex, i.e., lacking indentations, the shape of any particle is. It is also partially overlaps with to Circularity, but as an oval is not a circle but is convex, describes a separate shape component. Cuticle and structured organic material may be torn and thus be detected in Convexity. Convexity is measured as the ratio of convex hull perimeter to actual perimeter, from 0 to 1.
5. Intensity is calculated by how much light is scattered by a particle (Particle Characterization Guide, 2015); this can be used as a scale of light-colored particles to dark colored particles. Higher Intensity values are associated with darker colored particles such as amorphous organic matter, wood, coalified bits etc. and low Intensity values are associated with lighter colored particles such as cuticle pollen etc.

6. Solidity is the measure of the continuity of a particle or perforation of a particle, The more translucent a particle is the lower its Solidity value due to the software regarding this translucency as a perforation or hole in the particle (Particle Characterization Guide, 2015). Solidity is a similar measure to Convexity, but measures area 'missing' inside a particle outline. Convexity is measured as the ratio of area bounded by actual perimeter to the area bounded by convex hull perimeter as stated above. Solidity values vary from 0 to 1.

After running all the test case slides, the Malvern software was utilized to create dendrograms of these six significant morphological characteristics. The expectation is that for each sample, all three runs would cluster closer to themselves than to any other given sample. These test cases grouped to each other with very few exceptions across six variables of significance with regards to palynodebris. Because the MG3 does not specify the cluster algorithm employed, and does not create output files (e.g., .txt) to use, I constructed a MG3-based set of values for those six parameters using the mean and standard deviation for each parameter in each sample.

After examining consistency among light Intensity selections (result below), the MG3 method was further verified by comparing results produced by the MG3 and results from counts of palynodebris categories performed conventionally (by eye). This was accomplished by analyzing a set of twelve palynodebris slides from the MHF using the MG3 then comparing those results to the results collected by conventional means (in this case, by Dr. Richard Lupia). How well the relationship between these six parameters and those from a conventional analysis categories agree, reflected by consistent clusters of samples representing similar palynofacies, is

a measure of this method's success and applicability. Those twelve slides are from two separate sections of the upper member of the MHF but are contemporaneous depositional environments (Fig. 16). The slides position in the upper member of the MHF are important due to their association with vertebrate taxa collected from the same sediments.

Randomly picked slides (5µm or 10µm) from 12 samples were then analyzed with the MG3: samples OPC2409, OPC2412, OPC2416, OPC2427, OPC2433, OPC2434, OPC2437, OPC2440, OPC2442, OPC2453, OPC2454, and OPC2455. These twelve slides were run at 10x magnification with a light Intensity set at 70.00 and white balanced (Light Test 3). The SOP for each slide was done uniformly with the software's white balance setting and at the light intensity of 70. This is to provide a consistency to the analysis of these slides. The white balance setting was chosen because it provides the greatest amount of contrast between particulate matter and the background of the slide which allows the MG3 to take higher resolution images and consistently provided the highest particle counts in the "test" runs. After taking these measurements two-way dendrograms were created using the Past4 software using a paired group algorithm (UPGMA) and a cosine similarity metric.

To create this dendrogram the means and standard deviations of those six significant morphological parameters mentioned above. Except for Area (μm^2) which has values that will skew the results, all other parameters are measured from a 0 to 1 scale and are unit-less unlike the area measures. To compensate for that, the mean of the area measures were divided by the standard deviation of the area to produce a unit-less inverse coefficient of variation that will fall within the 0 to 1 scale on which the other variables are measured. A second dendrogram was created using data obtained from the analysis of those twelve slides done by hand by Dr. Lupia. The two dendrograms were compared, the first dendrogram derived from data taken from the

MG3 and the second dendrogram from the data collected by hand. An additional dendrogram was created using the ratios of palynodebris classes as percentages. Those classes are trilete spores, monolete spores, bisaccate pollen, *Classopolis* pollen, inaperturate pollen, monosulcate pollen, and eudicot pollen. This palynomorph class data were also added to both the data derived from the MG3 and conventional palynodebris analysis to better understand those groups. All dendrogram data were also arranged stratigraphically to determine any relationships of that data through time. This was performed to better understand the accuracy of both methods and to try to understand the correlation of the parameters that were measured by the MG3 to palynodebris types.

Results

Test Runs for Light Intensity Settings.

As stated above, in the test runs using three separate light and color settings, the particles counted for each sample were all had counts that produced a standard deviation of less than 5% of the particles counted, except for the three runs for OPC2461 which produced a standard deviation of 133,437 particles counted. The anomalous runs were included instead of the second three runs on OPC2461 to produce the dendrograms in Figure 7 in order to assess the accuracy of the data being collected and to better understand the limits of this method. The dendrograms that were produced from the test runs in which each slide was run under an SOP with different lighting and color settings all tended to group together with the exception of the low-count OPC2461 run in color mode run at a light Intensity of 75 (run 20). In the dendrograms in Figure 7. Runs 1-3 correlate to OPC2442, runs 4-6 to OPC2453, runs 7-9 to OPC2456, runs 10-12 to OPC2458, runs13-15 to OPC2459, runs16-18 to OPC2460, and runs19-21 to OPC2461. The

analysis settings for each sample are then delineated by (1), (2), or (3) representing each of the settings run for each sample.

The dendrogram for Circularity that the Malvern software generated is shown in Figure 7A. All three runs for each slide tended to group closely except for one run. OPC2461 (2) is graphed as an outgroup to all three runs of OPC2460 and not with nor close to OPC2461 (1) and (3). Also, the three runs of OPC2453 were close to each other, but successively joined to a cluster formed from OPC2442. In Figure 7B, which is a dendrogram comparing the Area (μm^2), all of the runs for each sample cluster together with the exception of OPC2461 (2) that sits in between the groupings of OPC2460 and OPC2461 (1) and (3). In Figures 7D and 7E, in which the standard deviation of the Intensity and Solidity of each sample are compared respectively, all runs for each sample cluster together with the exception of OPC2561 (2) which clusters all other samples than to OPC2461 (1) and (3).

Although a quick glance at each dendrogram reveals that OPC2461 (2) is repeatedly clustering with samples other than OPC2461 (1) and (3), the real pattern is the reverse, namely that OPC2461 runs (1) and (3) are distinct, usually very distinct, from all other samples. Graph C of Figure 7, which is the measure of differences in Convexity, shows consistent groupings of all runs with the exception again of OPC2461(2) which is grouped in the same cluster as OPC2460's three runs, but OPC2461 (1) and (3) are indeed joined to that cluster. A similar pattern is observed in the dendrogram comparing each run's Aspect ratio values in Figure 7F. Although samples are mixed together more than for other variables—OPC2460 and OPC2461 are intermixed as are OPC2453 and OPC2459—OPC2461 (2) is near OPC2461 (1) and (3). Most samples are dominated by elements with an Aspect ratio (width:length) near one ('equant' in conventional terms). In both Convexity and Aspect ratio, the lack of distinctness in (1) and (3) of

OPC2461 probably reflects the fact that equant elements tend to be circular and close in Aspect ratio of one. Thus the high number of measurements in OPC2461 (1) and (2), both over 300,000 elements, did not affect the means and so do not result in divergent samples. It is clear that this new method must compare samples with comparable number of measured elements to avoid spurious clustering.

This same issue—imaging comparable number of particles—arose again when investigating the randomly picked slides. A standard for the mesh size used to sieve pollen samples during processing is 10µm. When I originally randomly selected slides for the Morphologi G3 to analyze, I did not know there were slides that had been processed with a 5µm sieve. Four of the slides I had selected had been processed with a 5µm instead of a 10µm sieve. So I ran those four samples again with slides that had been processed with a 10µm sieve. In doing so, an anomalous result was obtained for OPC2427 that was labelled with a +10µm delineation. Multiple runs of that sample yielded particle counts above 900,000. This result was pulling OPC2427 towards the values of OPC2455 which is the sample in which no +10µm slide was available. OPC2455 consistently yields particle counts in the 500,000-600,000 range. All runs of the 10µm slides yielded particle counts in between 40,000-90,000 except for OPC2427. Reexamining the +5µm slide results, all particle counts were above 100,000, with OPC2453 and OPC2455 having the largest number of particle counts, 198,000 and 550,000, respectively. These high particle counts are expected for +5µm as the abundant fine material will pass through a 10µm sieve. However, the large number of particles being <10µm (Fig. 8) produces skewed results. Therefore, one should exclude not only kerogen but also 5µm-sieved palynology slides from this type of analysis using the Malvern Morphologi G3.

The anomalous result from the OPC2427 +10µm slide was still perplexing. So, I then compared it to the OPC2427 +5µm slide. The particle counts were wildly different, the +5µm slide yielded a particle count of 72,000 and the +10µm yielded a particle count of just over 900,000. I then decided to analyze the length and width graphs of each. In Figure 8 graphs 1a and 1b show the length and width percentages of all particles on a logarithmic scale for OPC2440 +10µm. There are two peaks on the graph the smaller peak in between 1µm and 10µm and the second larger peak being between 10µm and 100µm. In graphs 2a and 2b of Figure 8 the length and width trends of OPC2427 +5µm are shown to have a very similar bimodal distribution to the OPC2440 +10µm slide. Looking at graphs 3a and 3b from the same figure, OPC2455 +5µm is shown to have a single peak in between 1µm and 10µm in both graphs. The length and width distributions for OPC2427 +10µm can be seen in graphs 4a and 4b of Figure 8. As in OPC2455 +5µm the distributions contain one large peak in the range 1 to 10 microns and have a very low distribution above the 10µm range. This suggests that the labels for OPC2427 were swapped. After a quick analysis by hand of both slides from OPC2427 it does in fact appear that the slide labels were swapped during processing.

For the following results all slides processed with the Morphologi G3 were slides that have been processed through a 10µm sieve, except for OPC2455 in which there was no +10µm slide prepared. OPC2455 was still included in the analysis to illustrate the differences in results between +5µm slides and +10µm slides. Due to time restraints however, the hand counts include the four slides that were originally analyzed by the Morphologi G3 that were prepared with a 5µm sieve (noting that OPC2427 +5µm was mislabeled and therefore represents a slide prepared with a 10µm sieve). This may affect dendrogram groupings of the hand-counted slides that may

not be reflected in the dendrogram groupings of the samples analyzed using the Malvern Morphologi G3.

In the Area (μm^2) graph (Fig. 9A), all samples show bimodal distributions except for OPC2455 which exhibits a single peak between $10\mu m^2$ and $100\mu m^2$. This is expected due to the difference in sieve size during sample preparation. OPC2437 had the highest percentage of particles within the $10\mu m^2$-$100\mu m^2$ range with the next highest sample being OPC2434 followed by OPC2409. OPC2454 and OPC2453 have very similar curves, OPC2440 and OPC2412 also trend together. OPC2433 and OPC2427 have similar area values as well. Although there is no analog to measured area in the hand count categories, these data are pertinent to the determination of any taphonomic changes and can be used as a parameter in the identification of palynodebris types. The dendrograms in Figure 10 show the similarities of each sample using one parameter measured with the Morphologi G3. In graph A of Figure 10 the dendrogram for the Area (μm^2) of each MHF Formation pollen sample shows OPC2455 as an outgroup to all other samples which is expected because of the difference in sieve size for OPC2455 to the other samples. OPC2454 and OPC2453 are grouped together with a sister clade that contains OPC2440, OPC2437, and OPC2412. OPC2433, OPC2427, and OPC2416 are grouped together outside of the previous two groups. OPC2409, OPC2440 and OPC2434 make up a group that falls outside the three other groups.

Graph B in Figure 9 shows the Aspect ratio values for all twelve samples. OPC2453 had a large concentration of particles with Aspect ratio values close to 1.0. This suggests that most of the particles in OPC2453 are equant or rather that most of the particles found in OPC2453 are more equant than elongate. When compared to the hand-counted data, this trend is also seen, with more particles classified as equant than elongate with equant particles consisting of roughly

80% of the particles classified. All other samples cluster consistently below an Aspect ratio of 0.7 with the percentages of more equant particles increasing from 0.7 to 0.8 Aspect ratio range. Within that range however OPC2455, OPC2442, and OPC2416 have notably less particles in this range than do any of the other samples with their frequency curves dropping sharply as they approach an Aspect ratio of 1. Also of note, there is a spike in particle frequency at an Aspect ratio of 0.5 in OPC2455. That most particles lie above an Aspect ratio of 0.7 is also reflected in the hand counts as all samples have a higher concentration of equant particles in relation to elongate ones. In graph B of Figure 10 there are two distinct groupings of the Aspect ratio of the twelve samples. Within the first group OPC2454 is in a clade with OPC2437 the sister group to the first group contains OPC2442 as outside of a group containing OPC2427 and OPC2440. OPC2453 lies outside of those two groups. In the second group, two distinct families consist of OPC2409, OPC2412, and OPC2434 with the sister group consisting of OPC2433 and OPC2416 with OPC2455 found outside those two samples.

In graph C of Figure 9 the distribution curves for the Circularity value show that the sample with the highest concentration of particles that are close to circular (Circularity value between 0.9 and 1.0) is OPC2437. The samples with the next highest concentration of circular particles are OPC2454, OPC242 and OPC2453 respectively. The sample with the least number of circular particles is OPC2455. OPC2433 and OPC2416 have the next least number of particles in the 0.9 to 1.0 range. Of interest is the convergence of all samples on the Circularity value of 0.8. Except for OPC2409, OPC2434, and OPC2455 all samples only vary in their concentration of particles at the Circularity value of 0.8 by 0.05%. The convergence of nine of the twelve specimens at this value are indicative of specific palynodebris types, namely palynomorphs or amorphous organic material. OPC2409 and OPC2434 are markedly closer to the other sample

concentration at the Circularity value 0.8 than is the sample OPC2455. As stated above there is a particle size range discrepancy between OPC2455 and the other eleven samples that have been analyzed by the Morphologi G3. However, that relationship between size and Circularity is an unexpected result and may require more investigation to confirm. Circularity is likely tracking both palynomorphs and amorphous organic material within each sample.

Graph C of Figure 10 shows the Circularity similarities between all samples. There are three distinct groups that the dendrogram provides. OPC2455 and OPC2416 make up an outgroup to all the other samples. However, their difference values are higher to each other than any other two samples that are grouped together. OPC2454, OPC2442, and OPC2437 make up another group with OPC2437 sitting outside the group that contains OPC2454 and OPC2442. In a sister group that is further subdivided into two sample groupings that contain OPC2453 grouped with OPC2412, outside of that is OPC2427 and the sample outside of that grouping is OPC2434. The other group consists of OPC2440 grouped together with OPC2409, with OPC2433 outside that group.

The Convexity distribution graph found on graph D of Figure 9 reflects the distributions of Circularity however with a much more severe spike in convex particles between 0.9 and 1.0 after remaining relatively flat between 0.0 and 0.5 Convexity values which then gradually rise in concentrations across all samples between 0.5 and 0.9 before spiking sharply. OPC2455 has the lowest concentrations of convex particles, again this may be tied to the difference in preparation of the samples that is producing the curves that differ so much from the other samples. OPC2442 also has a relatively flat Convexity curve between the 0.9 and 1.0 Convexity values. OPC2440 and OPC2409 have the next lowest concentrations of convex particles respectively. The low values found OPC2442 and OPC2440 may be reflective of a stratigraphic relationship that will

be explored further below. OPC2437 has the highest concentration of particles between the Convexity value ranges of 0.9 and 1.0, followed by OPC2454 which has a difference of 0.8% to OPC2437 all remaining samples have a variable range of Convexity between 1.0% and 1.5%.

The Convexity dendrogram supplied by the Morphologi G3 grouped all twelve samples slide from the Moreno Hill Formation in three distinct groups. As in the Circularity dendrogram OPC2455 and OPC2416 are in a group outside of the other samples. However, the Convexity differences are much lower in this grouping than in the Circularity grouping. The first of the other two groups consists of OPC2454 and OPC2442 with OPC2434 lying outside of the group consisting of OPC2454 and OPC2442 and OPC2437 as the outside member of this group. The second group has two further groupings within it. The first group consists of OPC2427 and OPC2453 grouped together with OPC2412 outside of that grouping. That groups sister clade consists of OPC2433 and OPC2409 with OPC2440 sitting outside the group consisting of OPC2433 and OPC2409.

Intensity is a measure of the reflective properties of the particles, the higher the Intensity the more light is being absorbed by the particle therefore the darker the particles color. The Intensity spectrum can be used as measurement of color for each particle analyzed by the Malvern. The distribution of these values can provide information on the type of palynodebris material a sample is composed of and the percentages of dark palynodebris material (structured organic matter, wood, carbonized material, amorphous organic matter) and palynodebris constituents that are generally on the lower end of the Intensity spectrum (palynomorphs, cuticle amorphous organic matter). In graph E of Figure 9 the mean Intensity distributions for the twelve MHF pollen samples are shown. OPC2455 has the highest concentration of particles that would be considered dark. OPC2442 has the next highest percentage of dark particles OPC2440 and

OPC2433 have very similar concentrations of dark particles and particles on the lower end of the Intensity spectrum. OPC2453 has the highest concentration of lighter colored material. OPC2434 and OPC2416 have similar concentrations of lighter colored material and darker particles. These data reflect the hand counts of all the samples with similar concentrations of particles that are higher Intensity. Ratios of particles with lower Intensity are generally much lower than concentrations of particles with high Intensity values.

The Intensity dendrogram shows three distinct groupings of the MHF samples with OPC2455 as an outgroup to all other samples. OPC2442 and OPC2434 form a group with OPC2454 sitting outside of it. Outside of that grouping is OPC2412 with OPC2437 being outside of that grouping. In the second group OPC2453 and OPC2427 make a group with OPC2440 sitting outside that group and OPC2409 existing on the very outside of that grouping. The third cluster contains OPC2433 and OPC2416.

The Solidity measurement that the Malvern Morphologi G3 makes is a measure of the continuity of any given particle. The greater amount of perforation or gaps in the general shape of the particle the lower it's Solidity value. Because many constituents of palynodebris are translucent or have low amounts of opacity those particles exhibit low Solidity values whereas other palynodebris types such as structured organic matter (wood, carbonized material, amorphous organic matter) exhibits higher Solidity values due to the inability of light to pass through the particle. Therefore, this parameter can be used to measure the opacity of any given particle and derive information on the concentration of opaque and translucent particles within any measured sample. In graph F of Figure 9, OPC2455 OPC2433, and OPC2416 have the lowest concentrations of opaque particles. This can be observed in the data from the hand counted specimen of OPC2416 which exhibited a high amount of cuticle and light colored

structured organic matter. OPC2433 is anomalous, this is likely due to the difference in sieve size during preparation of the sample. As cuticle is generally larger than 10µm, all that material would be excluded in the OPC2433 +5µm slide. OPC2437 has the highest concentration of opaque particles with all other samples falling within a 0.8 % range of concentration of opaque particles.

The Solidity dendrogram in Figure 10E shows that there are three major groups with OPC2455 once again representing an outgroup to the rest of the samples. OPC2454 and OPC2437 make up a group with OPC2442 outside of that grouping and OPC2453 as an out member to that group. The sister clade of that group in this dendrogram consists of OPC2412 and OPC2427 as a very close group with OPC2409 outside of that group and outside that group of three specimens is OPC2434. OPC2416 and OPC2433 make up a group outside of the aforementioned groups, with OPC2455 being outside all other groups.

The dendrograms in Figures 11-15 were created using the Past4 application and analyzed using a unweighted pair group method using arithmetic averages (UPGMA) algorithm and a cosine similarity index to generate a two-way analysis of sample clusters and variable clusters, using Morphologi G3 palynodebris parameters, conventional hand count palynodebris data, and palynomorph (= pollen and spores) count data. The hand-counted data was normalized to 100 to mitigate the difference in total particles counted for each sample. In Figures 14 and 15 the percentages of each palynomorph class (which were counted by hand) were added to both the hand counted palynodebris data and the data collected from the MG3. In the case of the data collected from the MG3 the pollen class percentages were converted to numbers on a scale from 0 to 1 with the rest of the values collected from the MG3. For each dendrogram Figure, standard groupings are labeled A and stratigraphic relationships are illustrated in graphs labeled B. The

stratigraphically constrained dendrograms help visualize the changes for each parameter within the samples through time.

In Figure 11 the dendrograms derived from the data collected from the Morphologi G3 are shown. In Figure 11A three major groups are illustrated with OPC2455 representing an outgroup to all other samples. OPC2427 and OPC2433 make up a crown group with OPC2416 lying outside of that relationship. A sister clade within which two other sister clades are grouped contains OPC2442 and OPC24554 with very high similarities. Just outside of that grouping is OPC2434. The sample outside of that clade of three samples is OPC2437 with OPC2409 rounding out that group. The sister clade to that group contains OPC2440 and OPC2453 with OPC2412 being the out member to that grouping.

The parameters that appear to be most deterministic in the grouping of the samples analyzed by the Morphologi G3 are Area, Intensity, Convexity, Circularity, and Solidity. The generally broad spectrum of Area values has a significant pull on the relationships between samples this is illustrated by the placement of OPC2455 as its vastly different area pulls the sample away from the others. This behavior can also be seen in the Intensity and Solidity parameter as the values found in OPC2455 are much lower than in the other samples. It also appears that Convexity and Solidity have significant influence on the grouping of samples due to the relatively high values found within those parameters in relation to other values which generally fall below 0.7.

In Figure 11B, the changes in size of palynodebris can be seen through time. OPC2409, OPC2412, and OPC2416 show a decrease in area over time. OPC2427, OPC2433, OPC2434, and OPC2437 show an increase in particle size moving up through the stratigraphic section. The size drops again at OPC2440 and gradually increases through OPC2454, with OPC2455 having

the smallest area which is expected due to the sieve size used during preparation of the sample. Aspect ratio values increase among samples OPC2409-OPC2416, this pattern is also seen in OPC2427-OPC2434 with another drop in Aspect ratio found in OPC2453 which then increases again through OPC2454. No other obvious pattern can be found in the stratigraphically constrained dendrogram in Figure 11B.

The dendrograms in Figure 12 illustrate the relationships of the samples to each other in relation to the palynodebris data collected by hand. In Figure 12A, four major groupings of the samples are shown. In one group, OPC2440 and OPC2427 are shown to make a clade with OPC2433 sitting outside that similarity. OPC2416 is located as a sister member to that clade within the first group. In the second group OPC2434 and OPC2442 are very similar, and their group has a sister clade which contains OPC2412 and OPC2409 with OPC2455 as an out group to those two sister clades. This group also had the highest amount of elongate particles of all the samples. OPC2437 exists as a lone member of a group outside of the two afore mentioned major groups. OPC2454 and OPC2455 exist as their own group outside of the groupings of all other samples. The samples with the highest amount of terrestrial palynomorphs grouped together while other features of those samples have variable ranges of values. The grouping of OPC2454 and OPC2453 seems to almost entirely reliant on their very high percentage of amorphous organic matter (AOM) found within those samples. That OPC2416, the sample that has some of the highest values among all parameters, is grouped with the other samples with the highest palynomorph percentages. It may be that the values of AOM are so much higher in OPC2454 and OPC2455 that they pull those two samples together, and away from the other samples. No patterns related to stratigraphy can be determined from the palynodebris percentage values.

Figure 13 shows the clustering based on percentages of palynomorph types found within the MHF Formation samples. Trilete and monolete spores, *Classopolis*, inaperturate pollen, monosulcate pollen, bisaccate pollen, and monosulcate and eudicot angiosperm pollen grains are measured as a percentage of total pollen grains counted for each sample. This data distribution produces two major groups which contain five samples in each of those groups. OPC2434 and OPC2442 are in a clade with OPC2412 grouping outside of the close group. OPC2409 is mapped as a sister clade to that group of three samples. OPC2416 is outside of the clade that contains OPC2434, OPC2442, and OPC2409. The second major group shown in Figure13A consists of OPC2427 and OPC2433 being the most similar followed by OPC2440, OPC2455, and OPC2437 respectively. OPC2453 is outside of all other samples but is grouped together in relation to OPC2454. These groupings are driven by the high percentage of inaperturate pollen. The broad distribution of trilete spore percentages in the samples is contributing to the separation of OPC2453 from the other samples and the high percentage of bisaccate pollen in OPC2454 in relation to the other pollen types is pulling its grouping away from all other samples.

In Figure 14, the dendrograms show the data collected with the Morphologi G3 combined with the ratios of pollen classes found in each sample. The grouping in Figure 14A reflects the dendrogram in Figure 13A with a few key differences. OPC2453 has replaced OPC2455 in its relationship to OPC2440 and OPC2437. OPC2454 sits outside the grouping of the other samples and OPC2455 is the out group to all other samples. The broad distribution of data among pollen ratios is driving these groupings, so much so that they are almost identical. Only the extrema among the morphological features had any effect on the groupings with the vast amount of difference is OPC2455 being reflected in its placement as an outgroup. The stratigraphically constrain dendrogram in Figure 14B reflects the same patterns seen in Figure 12B, although now

with the added benefit of more refined ecological information tied to those patterns. An inverse relationship in the ratio of inaperturate pollen and area can be seen in samples OPC2409, OPC2412, and OPC2416. As the mean area of the particles decrease the amount of inaperturate pollen increases. In OPC2427, OPC2433, and OPC2434 there is positive correlation between these two parameters. Again however, in OPC2437, OPC2440 and OPC2442 there is an inverse relationship between area and inaperturate pollen. OPC2453 and OPC2454 exhibit a positive correlation between those two parameters. OPC2455 shows an inverse correlation but that is, if not intuitive, somewhat expected due to the difference in sample preparation from the other samples analyzed by the MG3. There is also an inverse relationship between Aspect ratio and inaperturate pollen occurrence.

The dendrograms in Figure 15 show the palynodebris data normalized to a scale of 100 combined with the hand counts of pollen classes. In Figre15A, three major groups of the MHF samples are shown. OPC2434 and OPC2442 make up a crown group with OPC2412 outside of that group. OPC2409 is the sole member of a sister clade to the aforementioned group. The second and largest cluster is sister clade to the first. OPC2427 and OPC2433 are the most similar samples followed by OPC2440, then OPC2455, followed by OPC2437. OPC2416 sits as an outgroup to all other samples within this major group. OPC2453 and OPC2454 make up the final group outside the relationships to all other samples from the MHF. These groupings are consistent with both the data derived from the MG3 combined with the pollen ratios and the dendrogram groupings of only the pollen ratios with a few exceptions. The position of OPC2416 is variable from both dendrograms. As in the dendrograms analyzed above it is the high ratio of inaperturate pollen in sample OPC2416 that pulls it away from the other samples that it has a

closer relationship with among other parameters. The high relative percentages of cuticle and light-colored particles OPC2416 also contribute to its position within the sample groupings.

Figure 16 illustrates the stratigraphy of the MHF and the stratigraphic position of the pollen samples analyzed, coded by cluster membership according to each data set. The consistent grouping of OPC2427 and OPC2433 among all methods suggest that among all parameters measured those two samples are derived from very similar depositional context and uniform pollen and spore flora despite the difference in the lithology of the two samples OPC2427 collected in a beige mudstone (fossil gleysol) and OPC2433 collected in a gray mudstone (fossil vertisol). The MG3 dendrogram and the hand-counted palynodebris dendrogram also grouped OPC2416 in that same cluster. OPC2440 is also included in the same group in the hand-counted palynodebris data. That these four samples have the highest concentrations of pollen and are grouped together in both the MG3 data (except for OPC2440) and the hand-counted data suggest that the environments of deposition were very similar but given that OPC2416 sits in a different group in relation to palynomorph class types that the biological components of those similar environments were very different. OPC2434 and OPC2442 also have consistent groupings across all three methods. The MG3 dendrogram groupings of OPC2434, OPC2437, and OPC2454 have consistent lithologies that match their grouping. OPC2442 however, was collected at the base of a beige mudstone which is different from the grey mudstone that characterizes the other samples. That OPC2409 and OPC2442 were collected at regions of lithologic transition and group together may also be significant. That OPC2409, OPC2412, OPC2416, OPC2434, and OPC2442 have similar concentrations of palynomorph classes suggest some kind of floral turnover in OPC2434 in relation to OPC2433. A similar trend is found in the relationship between OPC2440 and OPC2442.

Discussion

The variability of the parameters measured explain the inconsistency in the groupings. OPC2455 was prepared using a smaller sieve size and thus would be expected group away from the other samples when using the data from the MG3. That there are consistent groupings among the samples with the highest amount of pollen in both the hand-counted palynodebris parameters and the MG3-derived data supports the use of the MG3 to analyze palynodebris. While some of the groupings are inconsistent when related to the groupings derived from the other methodologies analyzed, there is some lithologic and stratigraphic consistency to the groups derived from the MG3 data. The larger amounts of data collected are likely a contributor to the differences observed in the dendrogram groups. That the parameters being looked at are also non-subjective also likely contributes to the differences in groupings among the different methods. The Area (μm^2) parameter is the most likely culprit for the differences in groupings as there is no analogous parameter in traditional palynodebris analysis. However as was illustrated above, samples that were prepared using a +10µm sieve exhibit bimodal size distributions. This is a result from smaller particles getting stuck on larger particulate matter and therefore remain in the sample despite the 10µm-mesh sieving. This will necessarily skew the mean values of Area (μm^2) as there will be many smaller particles (< 10µm) measured. This could drive the mean area of any given sample down, although that does not eliminate that variable's importance as most particles measured will still be above that 10µm threshold.

OPC2416 is consistently reported as the most dissimilar member of any group to which it is joined based on palynodebris. This positioning of OPC2416 is likely due to the large amounts

of cuticle and light-colored particulate matter. In dendrograms based on pollen and spore content, it is the high occurrence of inaperturate pollen that pulls it away from the other samples in its group. Notably, inaperturate pollen is characteristically also light to very light colored too.

The stratigraphic relationships of the Aspect ratio to the concentration of inaperturate pollen could be reflective of the amount of those pollen types in the dendrograms produced from the MG3 data. That there is inverse relationship between those two features would be consistent with more particles being less elongate in the samples that have a high occurrence of inaperturate pollen or of more pollen in general. Area is also a significant parameter stratigraphically as the mean size values can be correlated to lithology and the energy regimes those lithologies experienced during deposition.

The Intensity values represent color, the mean Intensity values are therefore reflective of the distribution of the color of particles in a sample. Those differences in color can then be used to estimate changes in the types of palynodebris in any given sample. This is best shown in OPC2416, which is full of cuticle and light-colored structured organic matter. The data collected from the MG3 shows this as a very low Intensity value the concentration of black material is expressed as higher Intensity values. OPC2455 is anomalous in this regard, however. That sample holds low Intensity values, but the hand counted data shows a much higher percentage of dark particles than light ones. The discrepancy in Intensity values is likely a function of the size of the particles analyzed by the MG3, the small size of the particles in OPC2455 inherently produce low Intensity values as they scatter less light. The optimal range of particle size that hardware analyzes is between 5µm and 500µm, perhaps at the very lowest end of its optimal range it may produce anomalous Intensity values. If that is the case, then the mean values of Intensity of all samples are unnaturally high and should exhibit generally lower Intensity values.

Although the values from +10μm samples are still valid as the higher number of large particles will still give a relative percentage of dark particles to light particles although perhaps not a true ratio.

The similarities of each cluster's members between the MG3 and conventional palynodebris analysis support the conclusion that the measurements collected by the Morphologi G3 are accurate and valid. The samples with the highest pollen concentrations grouped together likely because of the similarity in the parameters under which pollen would be measured by the MG3. Size [Area(μm^2)], color (Intensity), Circularity, and opacity (Solidity), all contribute to the grouping of those samples that have the highest amount of pollen. For the other groupings derived from the MG3 data the most important components appear to be size, color, opacity, and Convexity. The values of these parameters coincide with features present in palynodebris types.

The stratigraphic behaviors of the palynomorph classifications illustrate floral or taphonomic shifts through time. In OPC2409-OPC2416 there is an increase in the concentration of inaperturate pollen through time. This coincides with a decrease in eudicot pollen occurrence as well as a decrease in bisaccate pollen. Inaperturate pollen experience a pattern of increases in concentrations after sudden drops abundance. No stratigraphic pattern can be determined for the concentrations of trilete spores. The abundance of spores does appear to be tied to the amount of inaperturate pollen. Higher concentrations of inaperturate pollen are generally associated with lower concentrations of trilete spores. *Classopollis* also appears to be a significant contributor to the lowest concentrations of trilete spores in the samples. Because *Classopollis* is often an indicator of warmer temperature and sub-tropical climate (Vakhrameev, 1981) an inverse pattern with spores (trilete and monolete) that favor at least seasonal to persistent moisture and temperate climates is informative.

In the subsequent samples OPC2427-OPC2455 the relationship between spore concentration and *Classopolis* follow a similar pattern as OPC2409-OPC2416. OPC2453 and OPC2454 have the lowest concentrations of inaperturate pollen. OPC2453 has highest amount of trilete spores in any sample and OPC2454 has the largest amount of bisaccate pollen in any of the samples by a large margin. The vast difference in the floral constituents between OPC2453 and OPC2455 suggest heavy floral turnover within the same depositional environment, or it could represent a graded bed due to gradually decreasing energy. These differences are also reflected in the MG3 data which classifies each of these samples in different groups though they were collected in similar lithologies. This could be representative of some sort of climatic change or change in water supply as a fluvial channel moved more proximal to the area. These samples were collected in the top portion of a grey mudstone that is likely a fossil vertisol, given its color, that is topped by laminated sandstone which grades into a cross bedded sandstone. This is consistent with the sample from OPC2455 only being able to be run through a +5µm sieve. A farther distance transported before deposition would produce more mechanically worked palynodebris, breaking it down into smaller pieces. The smaller debris could also represent a lower energy environment than is found in OPC2453 or OPC2454. The increase in angiosperm pollen in OPC2455 may also reflect an environment with much more water as angiosperms can take advantage of a warmer wetter climate through their ability to quicky complete their life cycle to take advantage of those resources.

There is a significant difference in the floral assemblages between OPC2440 and OPC2442. There is a very low concentration of trilete spores in OPC2442 unlike OPC2440. However, there are much higher concentrations of *Classopollis* and bisaccate pollen in OPC2440 and OPC2442, as well as a higher amount of inaperturate pollen. OPC2442 was collected in a

beige mudstone that holds features of a fossil gleysol. Gleysols form in humid soils that have heavy inputs from alluvial sources which bring clay minerals and leach out other minerals such as calcium and iron. OPC2440 was collected in a gray mudstone which is a likely a fossil vertisol. Vertisols are typified by the high organic content and are typically found in ever wet environments. The organic matter is what gives vertisols their color (Kraus, 1999; Mack, 1992). The paucity of trilete spores in OPC2442 may indicate an environment that was relatively drier than the environment in OPC2440. The contrast of the beige mudstone (gleysol) where OPC2442 was collected and the gray mudstone (vertisol) where OPC2440 was collected indicate very different environments with different water regimes.

OPC2433 and OPC2437 exhibit high concentrations of trilete and monolete spores compared to OPC2434. The assemblage in OPC2434 may represent a change in water availability, this is evidenced by the concentration of *Classopolis* The presence of *Classopolis* has been used as a proxy for the temperature and aridity of an environment (Vakhrameev, 1981). It is however very resistant to mechanical weathering and oxidization, so is therefore prone to reworking. The presence of a high amount of elongate particles in OPC2434 would suggest that the palynodebris has not undergone significant decay or weathering. This would suggest that the presence of *Classopolis* in OPC2434 in much higher concentrations than in OPC2433 represent a shift in the climate within the same lithology. OPC2437 was collected in a gray mudstone in between a laminated sandstone layers which likely represents the migration of a fluvial channel proximal then distal then again proximal to the location. In the interstices of sandstone layers it is likely the environment had a constant supply of water. It is evident that some shift in environment occurred between OPC2433 and OPC2434. The larger amount of inaperturate pollen in OPC2434 along with the fewer spores may suggest an environment with less water than

in OPC2433 although the low amounts of angiosperm pollen in OPC2437 would not match this trend. The differences in all these samples are reflected in the hand-counted palynodebris dendrograms as well as the MG3 dendrograms. While OPC2434 and OPC2437 are often in the same major cluster, OPC2437 is often categorized as an outgroup to any group that contains OPC2434. OPC2433 is always grouped with the OPC2416, OPC2427 and OPC2440, the samples which contained the highest concentration of palynomorphs. While the difference of palynomorph classes are not directly measured by the MG3 their differences nevertheless are captured in the morphological parameter groupings.

Based on these stratigraphic relationships, the MHF Formation was a dynamic environment with variable floral successions through time. Those floral transitions are tied to slight shifts in climate and water regimes and are reflected in the shifts of groups like *Classopollis*, trilete spores, and eudicots. Inaperturate pollen, which can be used as a class of gymnosperm pollen, and trilete spore-bearing plants (ferns and allies) dominate the ecosystems represented by the palynodebris slides. The presence and concentration of certain classes of palynomorphs are dependent upon water availability with gymnosperms tending to be over-represented in environments with more restricted water regimes. Even within a single lithology these changes are shown to be dynamic, which is consistent with a nearshore floodplain whose water regimes are variable over time. These dynamic changes are reflected in the groupings produced by the MG3 data, which validates further exploration and use of this methodology to analyze palynodebris.

Conclusion

The purpose of presenting this methodology was to propose a new and quick way to analyze palynodebris specimens. That the Morphologi G3 produces data that is valid and pertinent to the classification of palynodebris types is illustrated in the distinct groupings that were shown in the dendrograms of Figure 9. The minor inconsistencies among those groupings when compared to dendrograms derived using traditional analysis techniques are likely a function of the differences in the types of data collected (raw morphometric measurements versus subjective classifications without measurements) and in the sieve sizes used for some of the samples that were hand-counted. OPC2412, OPC2433, OPC2453, and OPC2455 were all prepared using a +5µm sieve. This likely affected the groupings of the samples based on conventional 'hand' counts. Given the consistent dissimilarity of OPC2455 in the MG3 data and the variability found in both slides from OPC2427, sieve size during sample preparation significantly influences the data collected from the MG3 analysis. More development of the methodology needs to be conducted and will be discussed further below.

The standard operating procedure to use this methodology requires the use of the Malvern Morphologi G3 and its associated software (v8.11). It is possible that previous or subsequent versions of the software would be equivalent, but this needs to be verified.

1. use the software to create a new SOP. This is found under the file tab under "New." The software will then open a user window in which several analysis parameters can be adjusted.

2.Under the sample analysis tab in the user window, you can specify what kind the type of sample carrier to use in the analysis. Select the four-slide sample carrier and specify that there is a cover slip present on the samples. Be sure to select the option to generate separate analyses for each sample.

3.The next parameter to adjust is the scan area. This tab will show a picture of a slide (Figure 5.) and an adjustable green square which represents the scan area. The green square can be moved and adjusted in area. By clicking and holding on the slide you can drag the mouse to create additional scan areas adjust the size and position of the scan area rectangles until you form a transect as in Figure 5. Remember to compensate for labels covering a portion of the slide. The time total time for analysis should read between 18 and 22 minutes (otherwise reduce sizes of scan areas).

4. Under the light settings it is best to use the default setting of light Intensity at 80 but the user can adjust light Intensity as needed if there are other ambient light sources nearby that may affect the results.

5.Under the scan threshold tab, set the scan threshold to 195 which appears to be the best threshold to analyze palynodebris, although again this parameter can be adjusted as needed by the user.

6.Click “OK” on the SOP window and the software will prompt you to save the SOP. Once the SOP is saved prepare the MG3 to run the SOP.

7.In the four-slide sample carrier, mount slides that have been prepared with a +10µm sieve with the desired area of analysis on the right with the thicker edge of the sample carrier. This is the orientation locked in during the scan area portion of the creation of a new SOP.

8.Once the slides are loaded in the sample carrier click the load sample icon on the tool bar at the top of the screen, indicated by a green arrow.

9.Once the sample carrier is loaded click the file icon with a gear on it, this is the “Run SOP” icon. Click on it and select the saved SOP that you created earlier.

10. In new window the SOP can be started by hitting the start icon. The software then prompts you to delineate how many slides in the sample carrier will be analyzed using this SOP.

11.Select all relevant slides. The MG3 will then begin to calibrate but the user needs to do the initial focusing manually.

12.Once an acceptable focus is obtained, click the “Focus OK” icon in the bottom right of the window. The window will then transition to the light settings.

13.Select color mode, and then white balance as is seen in Figure x. Click “Light Ok” at the bottom right corner of the window. The window will then transition to a threshold settings screen.

14. Adjust the threshold as desired, the 195-threshold setting that was set during the creation of the SOP should be sufficient however. Click the “Threshold OK” icon on the bottom right of the window. The MG3 will then calibrate once more and begin the analysis.

15.Once the analysis is complete the relevant graphs can be produced under the Malvern “Default” statistics setting and the “Other Reports” statistics setting. Make note of the sample delineation and the position it was in on the sample carrier. Samples on the bottom of the sample carrier will be listed as the Run 1 in the software with Runs 2-4 moving up the sample carrier.

16.The runs can then be compared by highlighting them in the records tab and then clicking on the comparison tab. Dendrograms for each parameter can be viewed in this tab. For graphs, mean values and standard deviation values of the relevant parameters highlight any given run and click on the tab with the desired parameter. Comparison can

also be made by highlighting multiple runs and then clicking on the tab with the desired parameter.

Chapter 4

SYNTHESIS AND FUTURE WORK

The wood from the lower member of the MHF exhibits features consistent with some degree of water stress. The presence of coal seams throughout the lower member and the weakly pedogenic mudstones found throughout the lower member suggest that the availability of water was not the root cause of that water stress. Those features could have been caused by oversaturation of water that those individuals experienced in life, though it is far more likely, given the climate of the time that the evidence of water stress found in the wood from the lower member of the MHF are due to warm temperatures. High temperatures even in ever wet climates cause an increase in evapotranspiration, which can cause individuals to express features of growth that are similar to growth features found in plants living under drought conditions. So, while these individuals had a constant supply of water the climate in which they lived was likely extremely hot.

The high occurrence of coals in the lower member as well as a marine incursion at the base of the MHF (Kelley, 1987), suggest the Western Interior Seaway was far more proximal to the MHF during the deposition of the lower member. That proximity was likely a large contributing factor to the water regimes throughout the lower member. That high variability in climate is reflected in the growth series of two of the specimens collected from the lower member, OPC2462, and OPC2465. These woods would have grown in soils that were generally more saturated with water which could have induced the growing stresses found in both OPC2465 and OPC2462. There are larger logs of OPC2462 that were not collected in the lower

member of the MHF that should contain more complete growth series to further analyze the water regimes on small time scales.

The wood from the upper member of the MHF exhibited a more regular pattern of growth. This could be due to the generally drier conditions that are recorded in the upper member. Though the upper member was drier than the lower is evidenced by the lack of coals throughout the upper member, with the exception of a few coal seams near the base of the upper member. The mudstones found in the upper member are weakly pedogenic and represent the same types of fossil soils found in the lower member. While drier than the lower member, the upper member was by no means dry. The fossil vertisols and gleysols found in the upper member are consistent with soils found in similar environments today, poorly drained weakly pedogenic soils are often found in near shore and prodelta environments today. The growth features exhibited by OPC2469 may be indicative of a cooler climate than the sediments in the lower member represent. The weakly pedogenic mudstones of the upper member suggest intermittent depositional events, likely from seasonal influxes in water (floods), which reset pedogenesis to time zero. Those fossil soils also suggest a relatively constant supply of water as vertisol and gleysols are generally poorly drained. The differences in growth habit are therefore most likely controlled in this environment by temperature variation.

The high variability of environments shown in the analysis of the palynodebris from the upper member of the Moreno Hill Formation illustrate the dynamic near shore environment and the variability of water regimes found throughout the section. Although the environment was humid and the water supply was high throughout, the upper member was generally more arid than the lower member. The absence of coals throughout the upper member of the MHF are consistent with an environment that was more elevated relative to base level than the lower

member. The presence of (poorly developed) fossil soils throughout the section suggests there were lags in major depositional events that allowed some minor pedogenesis to occur. The gray mudstones exhibit minor pedogenic features throughout except for the gray mudstone in which OPC2437 was collected. The high amount of bisaccate pollen in that sample may suggest that the floral constituency was driven by wind pollinated plants which could mean that OPC2437 was likely ponded water rather than representing a zone of pedogenic activity. This relatively drier environment than the lower member is also reflected in the features related to climate in the fossil wood specimen OPC2469. The more regular growth seasons and the lack of intraseasonal growth rings supports the conclusions drawn by Cilliers et al. (2021) that the upper member represents a period in the history of the MHF in which the Western Interior Seaway was retreating away from that depositional center.

The shifts in climate recorded in the MHF correlate to a regression of the Western Interior Seaway. There is however no isotopic shift found in sediments thought to be of similar age to MHF in the sediments of the Western interior Seaway. While the age of the MHF has been recently further refined using detrital zircon analysis by Cilliers et al. (2021) it may be possible to further refine the age of the MHF using magnetostratigraphy.

With the MHF being deposited during the transition from the late Turonian into the earliest Coniacian, these terrestrial deposits can also be correlated to a shift in the earth's magnetic field polarity which has recently been reported during this period of sedimentation (Guzhikova et al., 2020, 2019). While the evidence of this reversal has not been rigorously analyzed in relation to the study area, it has been measured and analyzed in Russian sediments of similar age, namely the Ozerki-Lipovka sections of the Ryazan-Saratov trough. It should be noted that the reverse polarity measured in the Ozerki-Lipovka sections is anomalous with

regards to other proximal study sections, the Kimmenyi Brod and Nizhnyaya Bannakova, which exhibit normal magnetic polarity that is consistent with the GPTS (Geomagnetic Polarity Time Scale) with the exception of the Kimmenyi Brod section which yields no magnetostratigraphic evidence from that duration of time (Guzhikova et al., 2019). The duration of the reversal polarity zone within the Ozerki-Lipovka section spans from the Late Middle Turonian through the Coniacian and into the Santonian, which is inconsistent with the GPTS but does share similar polarity shifts with the GMSS (General Magnetostratigrahic Scale) (Guzhikova et al., 2020, 2019). By correlating paleomagnetic data from the MHF to the reversal found in Russian sediments of similar age it may be possible to either ratify this polarity shift or discount it.

The use of the Malvern Morphologi G3 to analyze palynodebris resulted in distinct groupings based on the raw morphometric measurements obtained through its use. To increase the applicability and accessibility of using the MG3 to analyze palynodebris slides further refinement of the method is necessary. Within the software the user can create classes that the software will use to categorize different particle types. By further analyzing the results particle by particle it may be possible to further refine palynodebris types by the range of values that those palynodebris classes share. For example, terrestrial palynomorphs should have typical ranges of Area(μm^2), Intensity, Circularity, Aspect Ratio, Convexity, and Solidity. By refining the range of each of those values a class can be created within the software that will group all particles within those ranges of values into the class that the user has created. This should be true for all palynodebris types. Structured organic matter may be expected to have higher Aspect ratio values and higher Intensity values, amorphous organic material can have a broad range of Intensity but has generally higher values of Circularity and could have low or high values of Solidity. Cuticle has low Solidity values and very low Intensity values. So, by analyzing the

features of each particle type a classification system using those parameters can be created using the MG3 software. These classifications can then be applied to records of samples that have already been analyzed by the MG3 and the percentages of each class can then be viewed for any sample that has already been analyzed and any future samples. Once those class concentrations have been measured in the existing data sets, I believe the dendrogram groupings using those class concentrations will more closely match the dendrograms generated using data from conventional palynodebris analysis.

These data could also be applied to an image recognition software a la Weller (2004). The MG3 also captures images of each particle though at very low resolution. With a newer machine, the Morphologi G4, higher resolution images will be produced. Those images can then be used to train an assisted neural network to classify palynomorphs at a much higher resolution than is possible with the current hardware. The vast number of data collected by the Morphologi G4 will also speed up the process of training the assisted neural network because any given sample run can generate tens of thousands of images of palynodebris. As it stands the MG3 produces significant results in a very short amount of time. Further development of this method will only improve its usefulness as a tool to analyze palynodebris.

FIGURES

Figure 1. Map of the Moreno Hill Formation and the Atarque Sandstone Formation. Study area is circled in red.

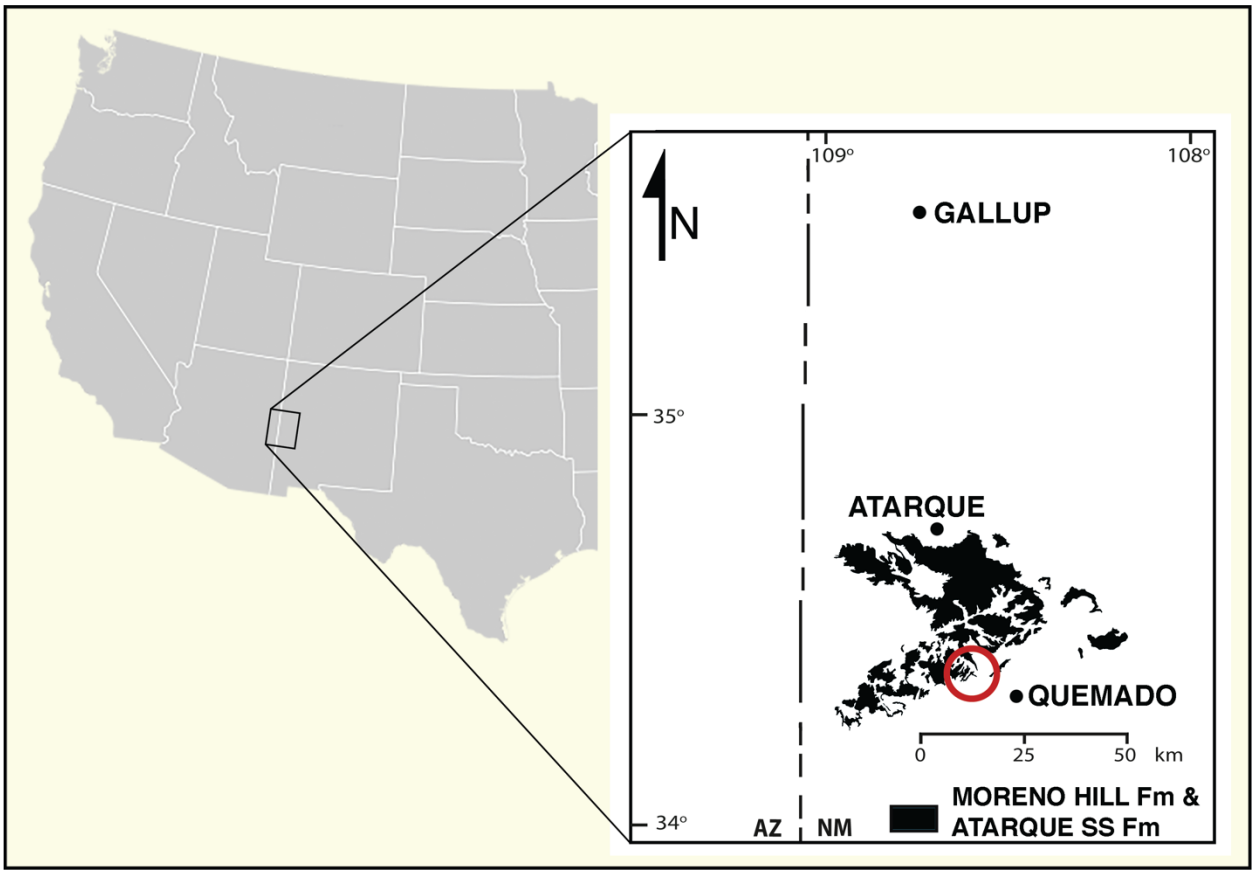

Figure 1B. Generalized local stratigraphy of the Moreno Hill Formation.

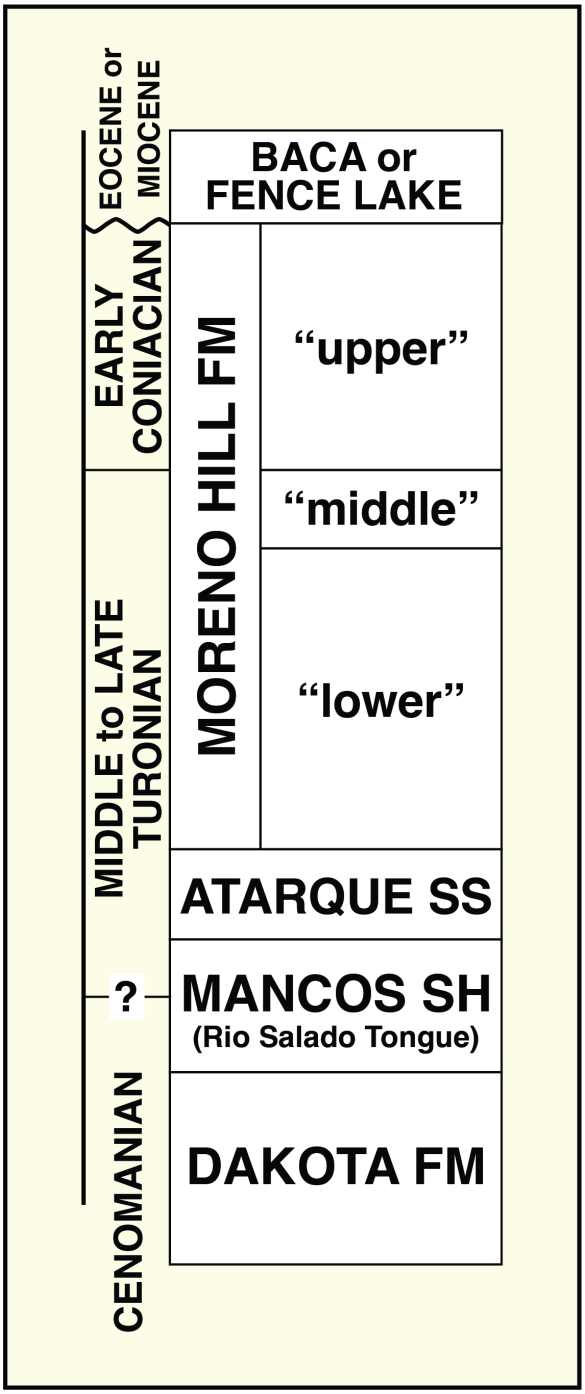

Figure 2. Field pictures of wood analyzed in this study. In (3) a large uncollected log is shown.

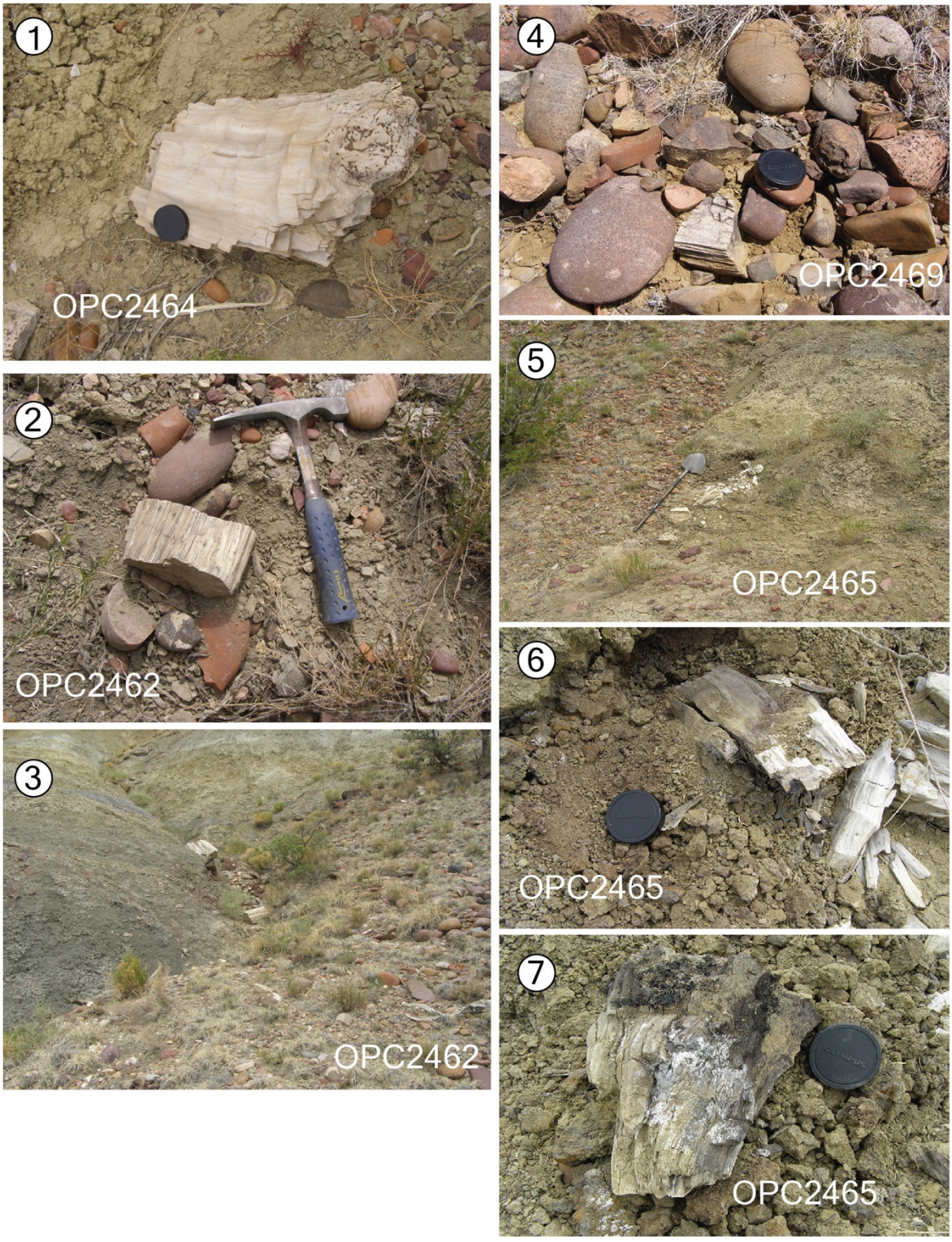

Figure 3. Generalized stratigraphy of the Moreno Hill Formation and relative locations of wood studied. (Modified from Cilliers, et al., 2021)

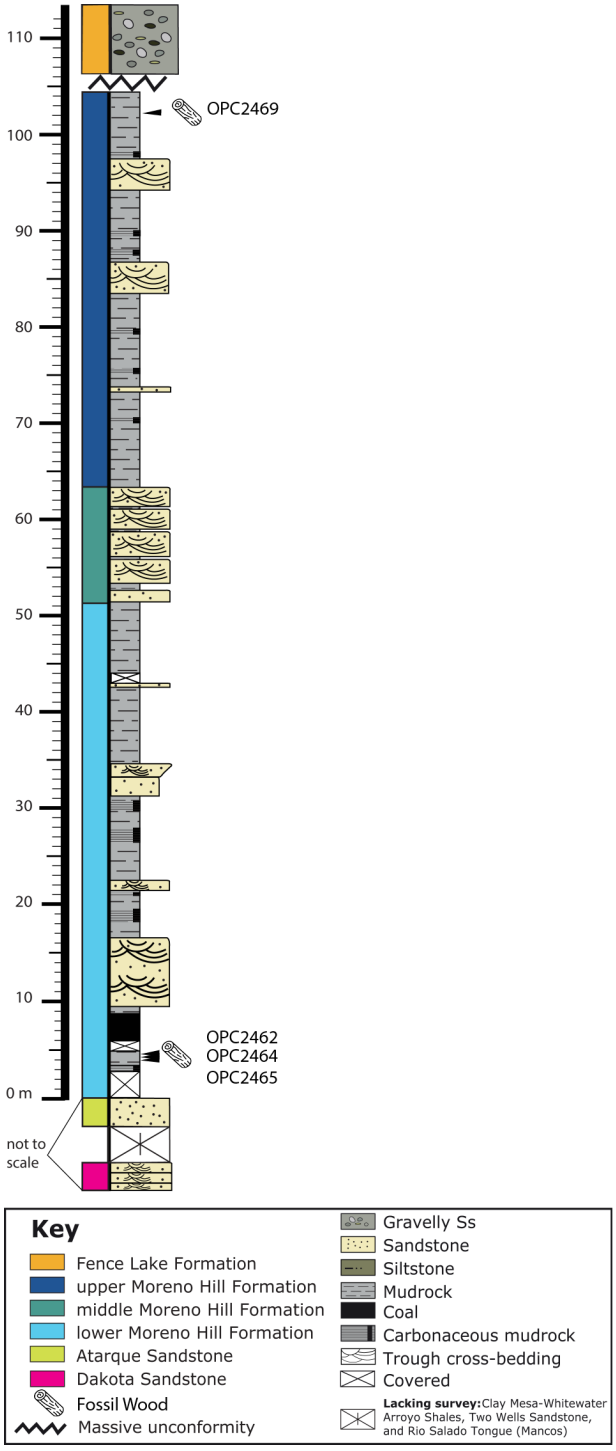

Figure 4. Images of growth series for Moreno Hill Formation specimens OPC2462, OPC2465, and OPC2469. Red arrows demarcate intraseasonal growth rings. Black arrows indicate seasonal growth rings. Scale bars 2000µm

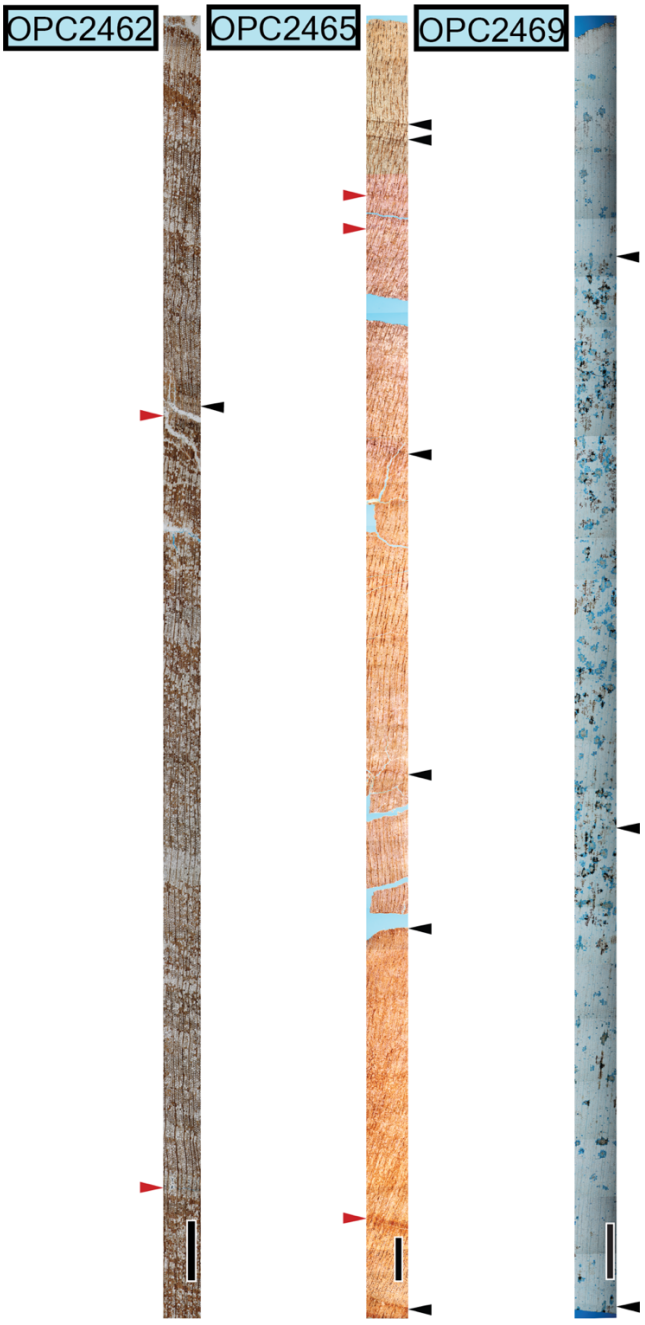

Figure 5. The Malvern software (v8.11) SOP editor window with the scan area editor shown to illustrate how to create a transect using the software.

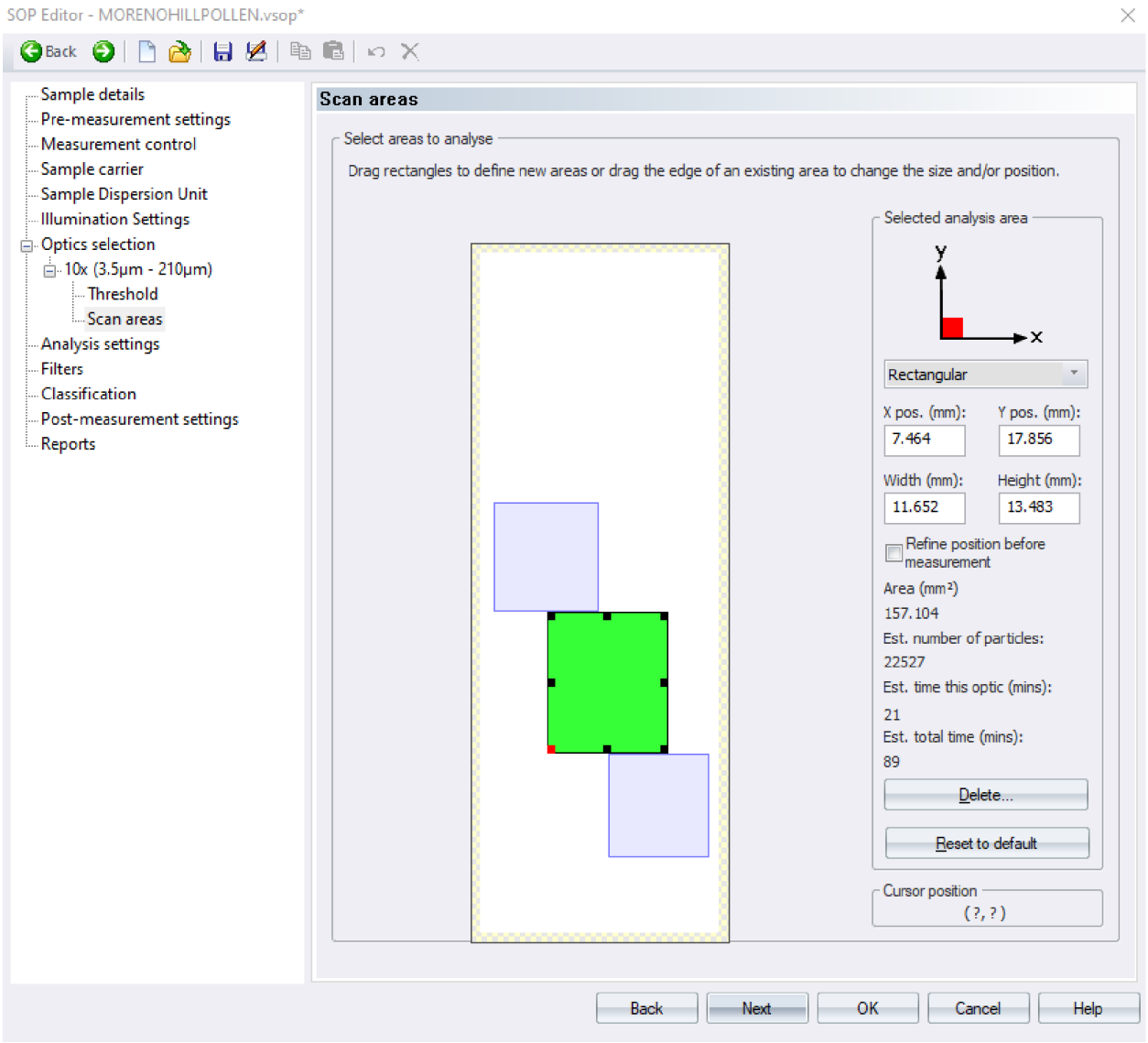

Figure 6. Malvern software (v8.11) interface showing the three different analysis settings used to analyze the test samples.

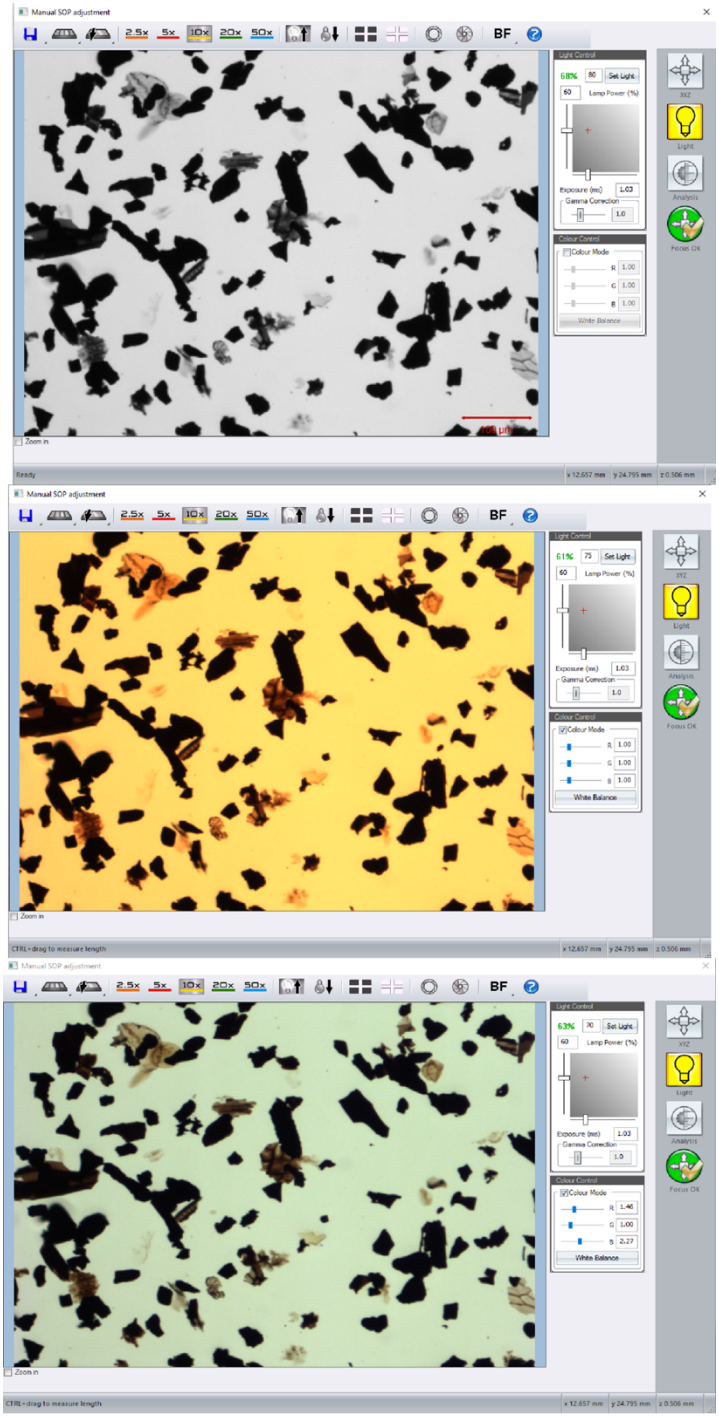

Figure 7. Test case dendrograms to test validity of software data outputs. Numbers beside slide names indicate the light settings under which they were run according to (1) Greyscale, Light intensity 80, (2) Color Mode, Light Intensity 75, (3) Color Mode White Balanced, Light Intensity 70. Dendrogram A: Area (μm^2). Dendrogram B: Aspect ratio. Dendrogram C: Circularity. Dendrogram D: Convexity. Dendrogram E: Intensity. Dendrogram F: Solidity.

A

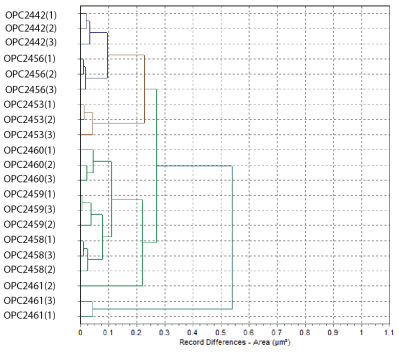

B

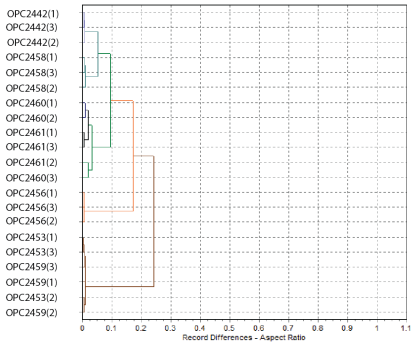

C

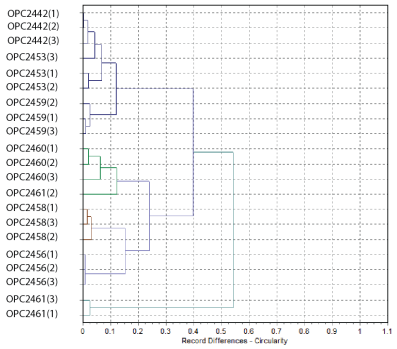

D

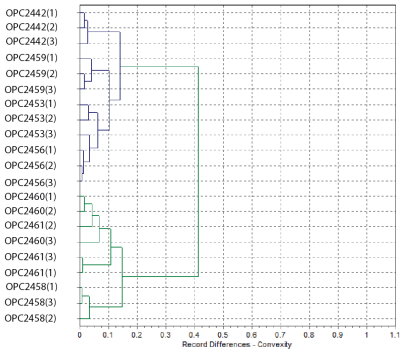

E

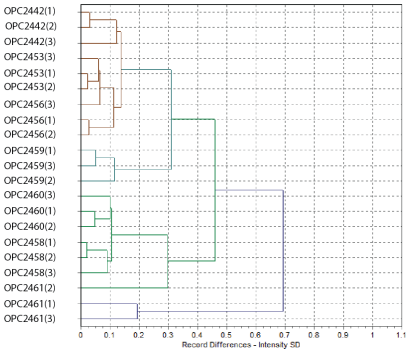

F

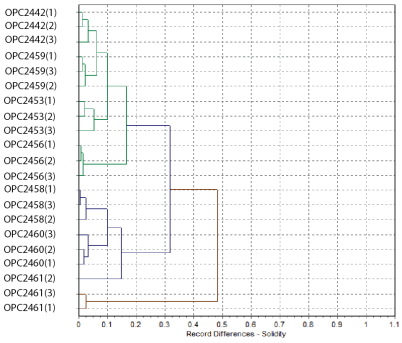

Figure 8. Length and width graphs of OPC2427 prepared with a +5µm sieve and a +10µm sieve compared to two other samples prepared with those sieve sizes. Graphs 1a and 1b: OPC2440 +10µm) length and width. Graphs 2a and 2b: OPC2427 (+5µm) length and width. Graphs 3a and 3b: OPC2455 (+5µm) length and width. Graphs 4a and 4b: OPC2427 (+10µm) length and width.

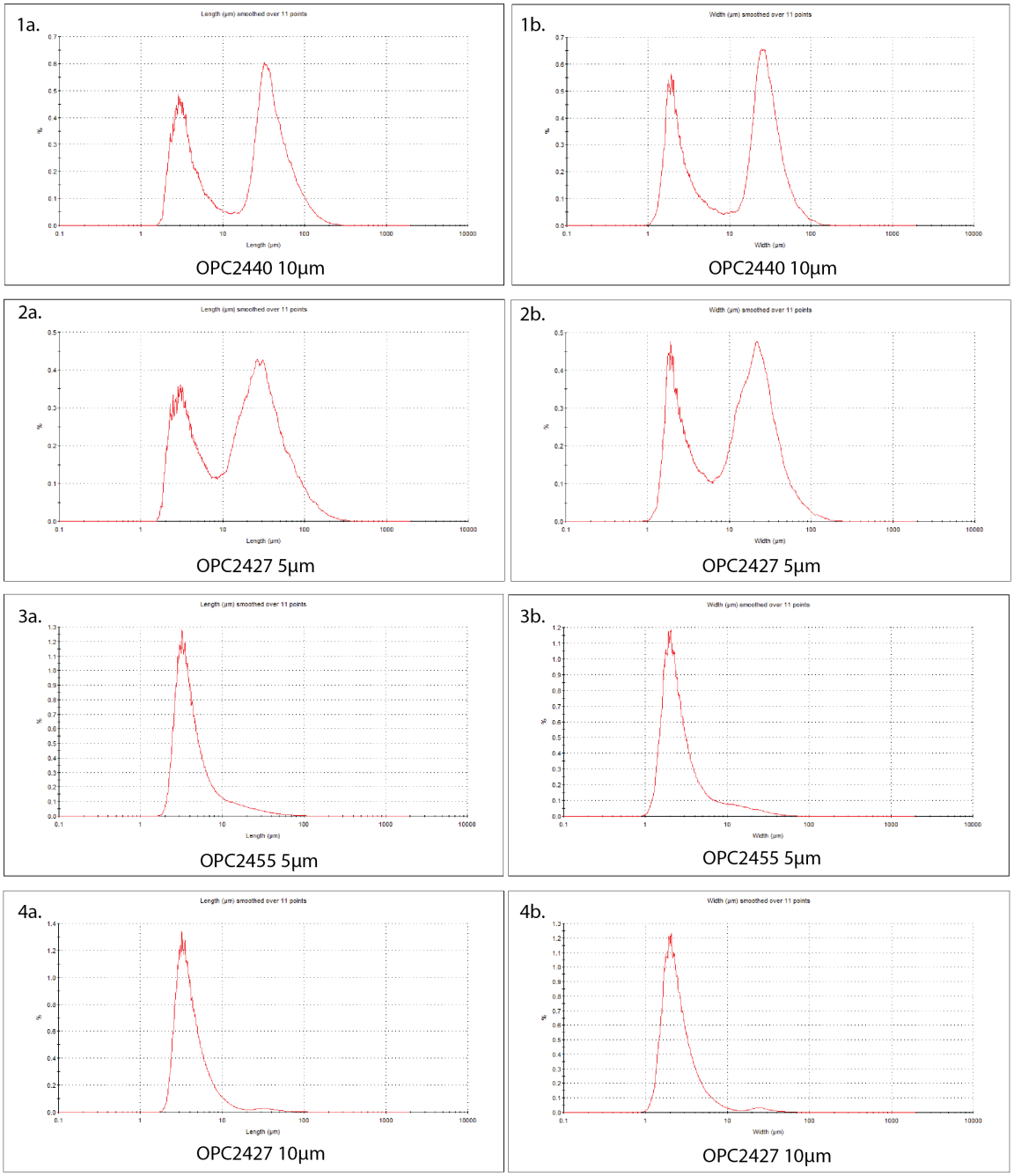

Figure 9. Comparison graphs of the MHF samples using the six parameters of importance to palynodebris analysis. Graph A: Aspect ratio. Graph B: Area (μm^2) Graph C: circularity. Graph D: Convexity. Graph E: Intensity. Graph F: Solidity.

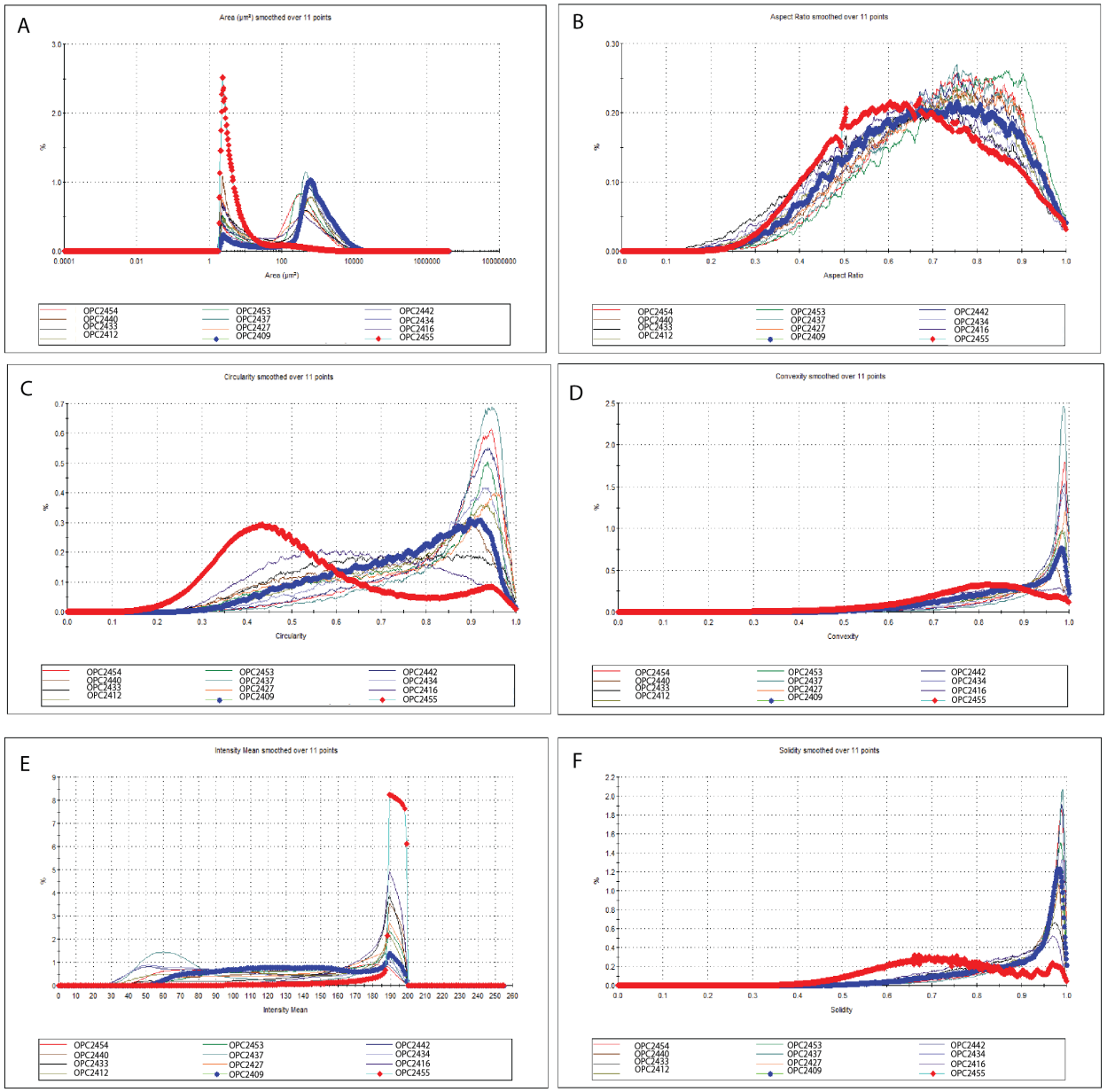

.

Figure 10. Dendrogram groupings for each parameter measured and generated by the Morphologi G3 software. Dendrogram A: Area (μm^2). Dendrogram B: Aspect ratio. Dendrogram C: Circularity. Dendrogram D: Convexity. Dendrogram E: Intensity. Dendrogram F: Solidity.

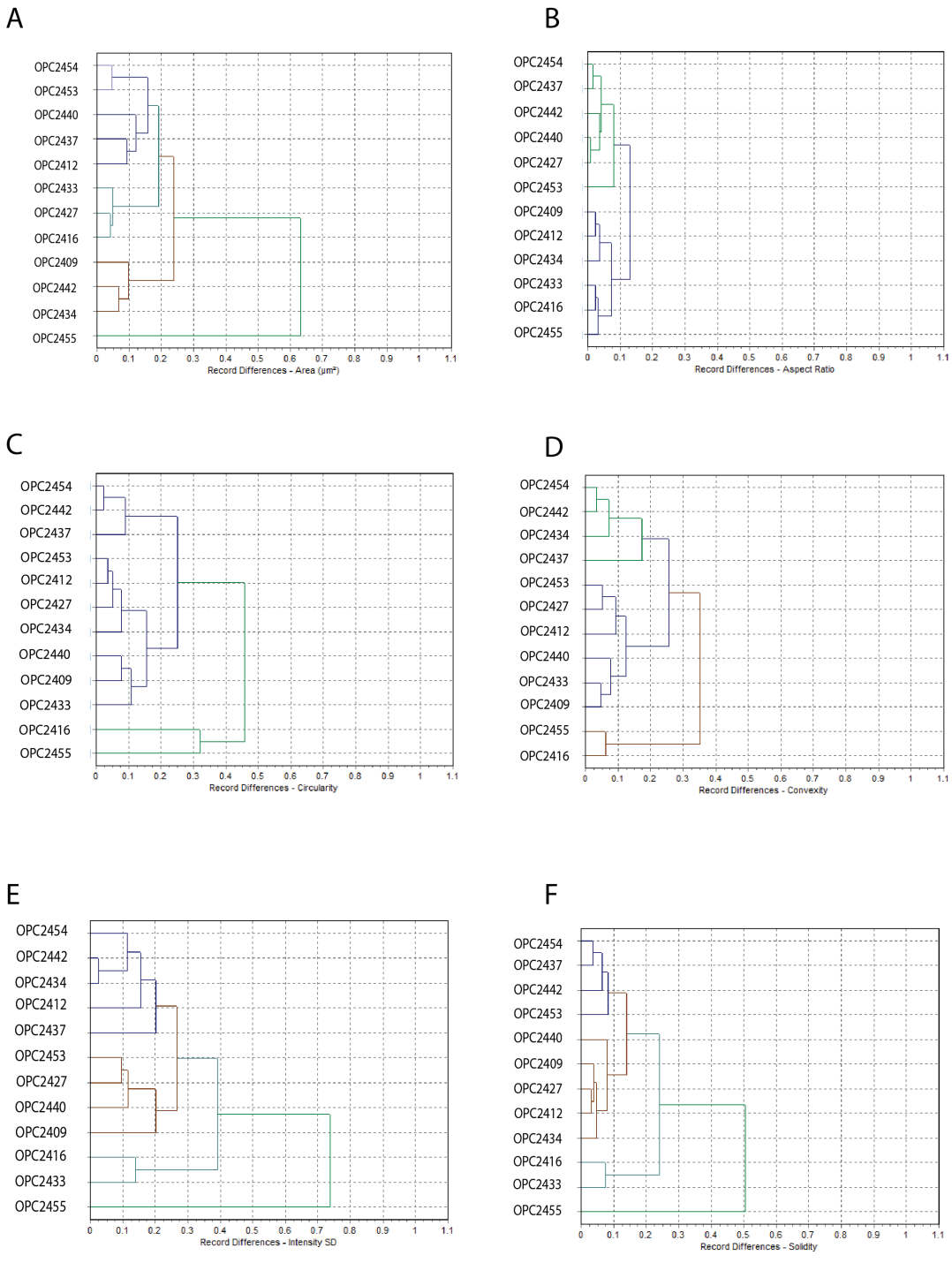

Figure 11. A: two-way dendrogram generated using the mean values and standard deviation values of the parameters significant to palynodebris analysis for each MHF sample. B is stratigraphic representation of those values for samples from lowest (OPC2409) to highest (OPC2455) in section. Made using Past4 software.

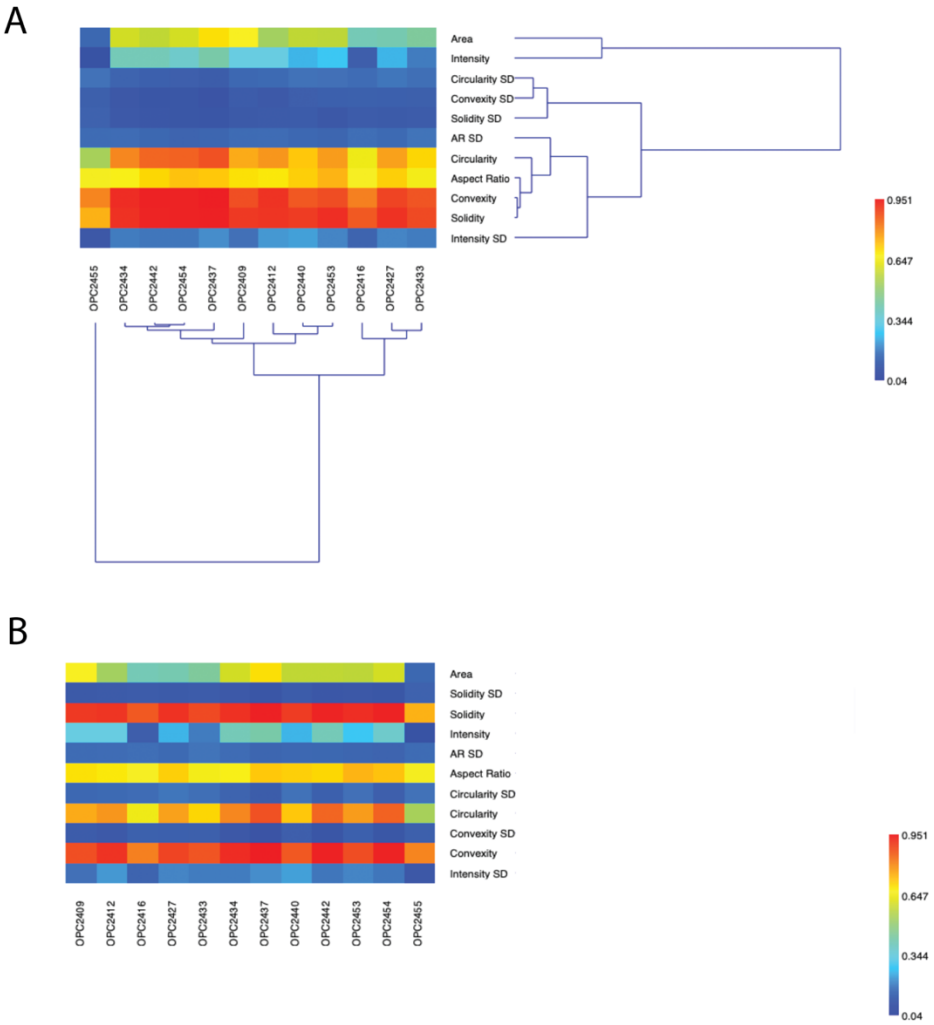

Figure 12. A: a two-way dendrogram analysis using conventional palynodebris data B: Stratigraphic representation of those values for samples from lowest (OPC2409) to highest (OPC2455) in section.. Made using Past4 software.

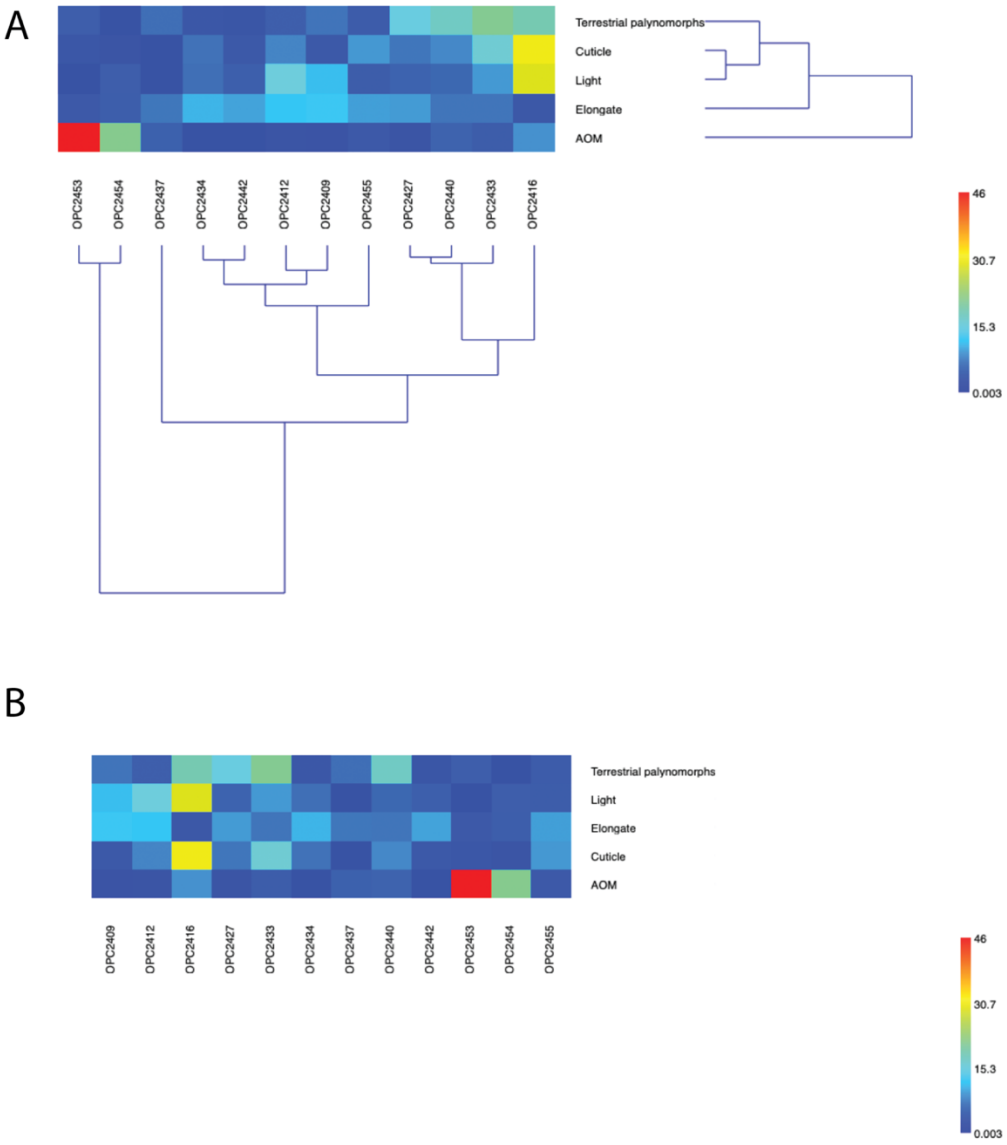

Figure 13. A: Two-way dendrogram generated using the palynomorph class data. B: Stratigraphic representation of those palynomorph classes for samples from lowest (OPC2409) to highest (OPC2455) in section.. Made using Past4 software.

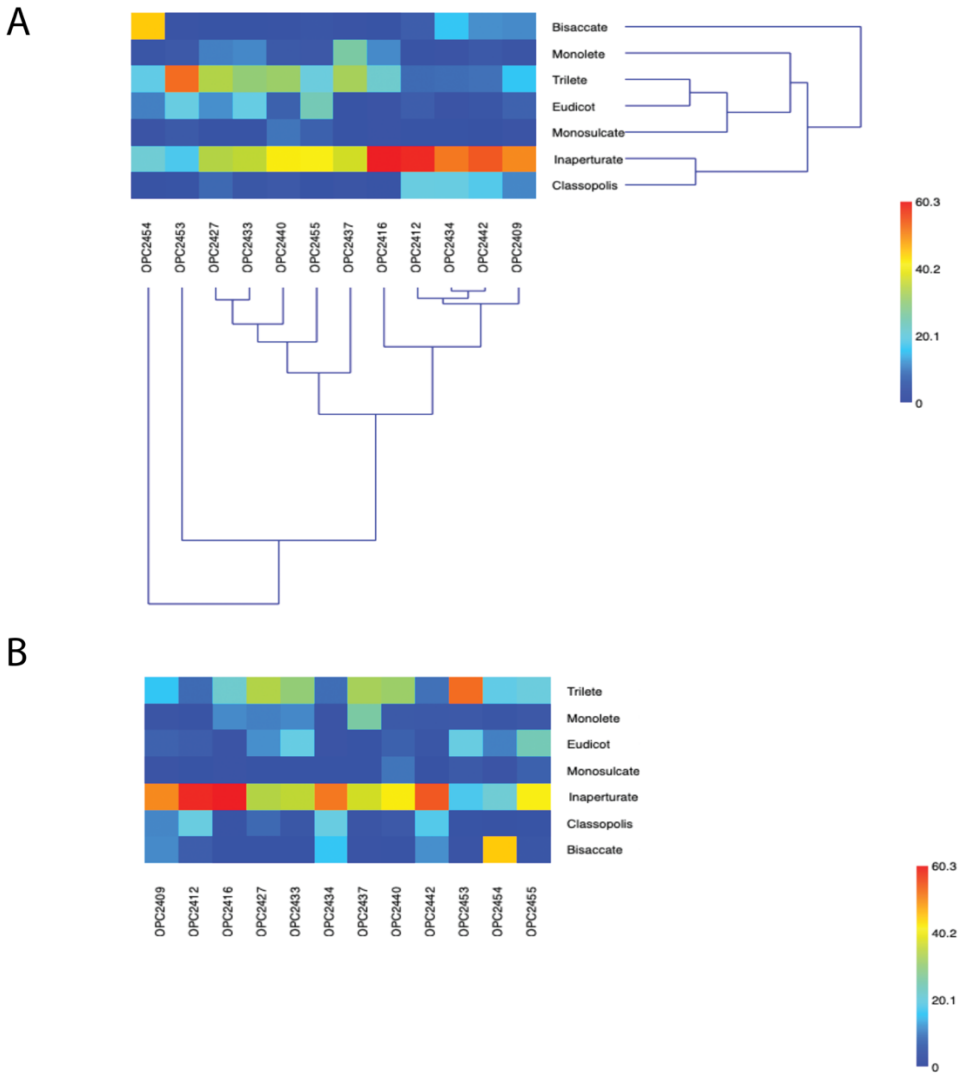

Figure 14. A: Two-way dendrogram generated using a combination of the data from the MG3 and the palynomorph class data. B: Stratigraphic representation of that data for samples from lowest (OPC2409) to highest (OPC2455) in section. Made using the Past4 software.

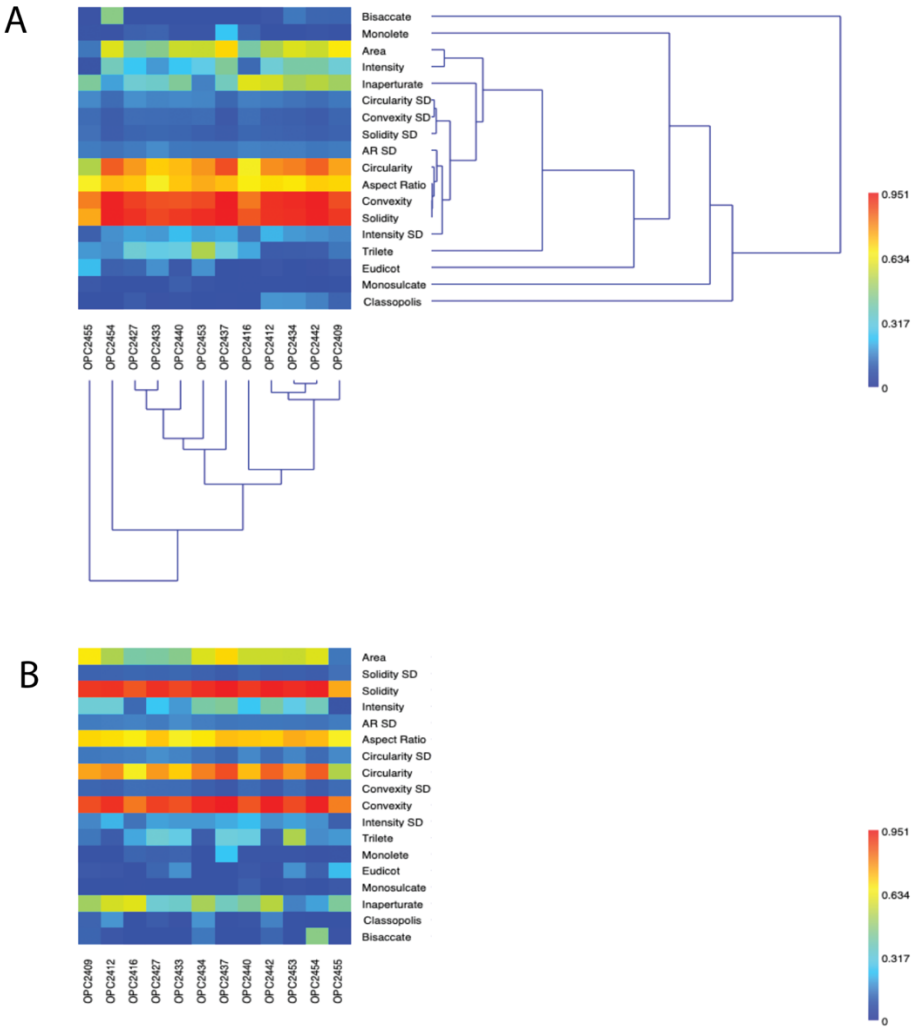

Figure 15. A: Two-way dendrogram using a combination of the conventional palynodebris data and the palynomorph class data. B: stratigraphic representation of that data for samples from lowest (OPC2409) to highest (OPC2455) in section. Made using the Past4 software.

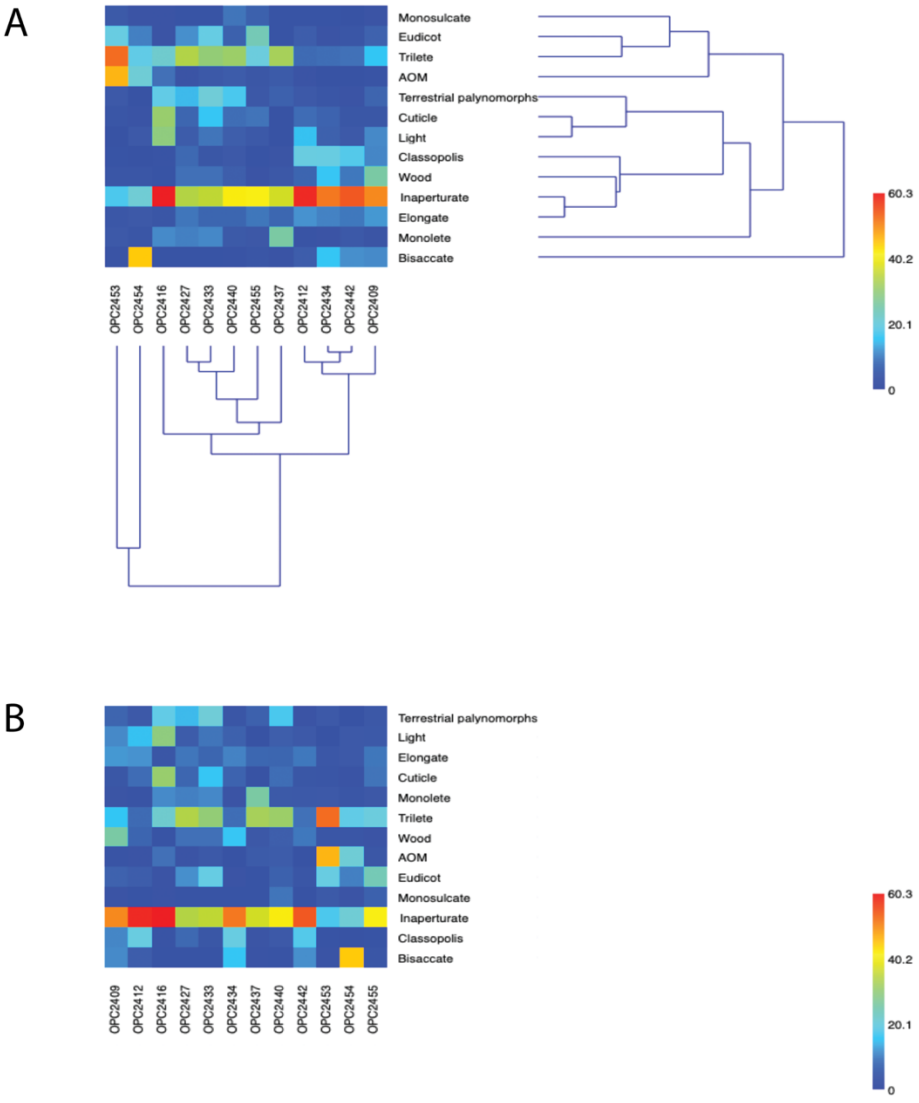

Figure 16. Stratigraphic sections of the upper member of the MHF with the locations of the pollen samples that were analyzed using the MG3 and conventional methods. Higher intensity symbol colors indicate consistent groupings among different methods.

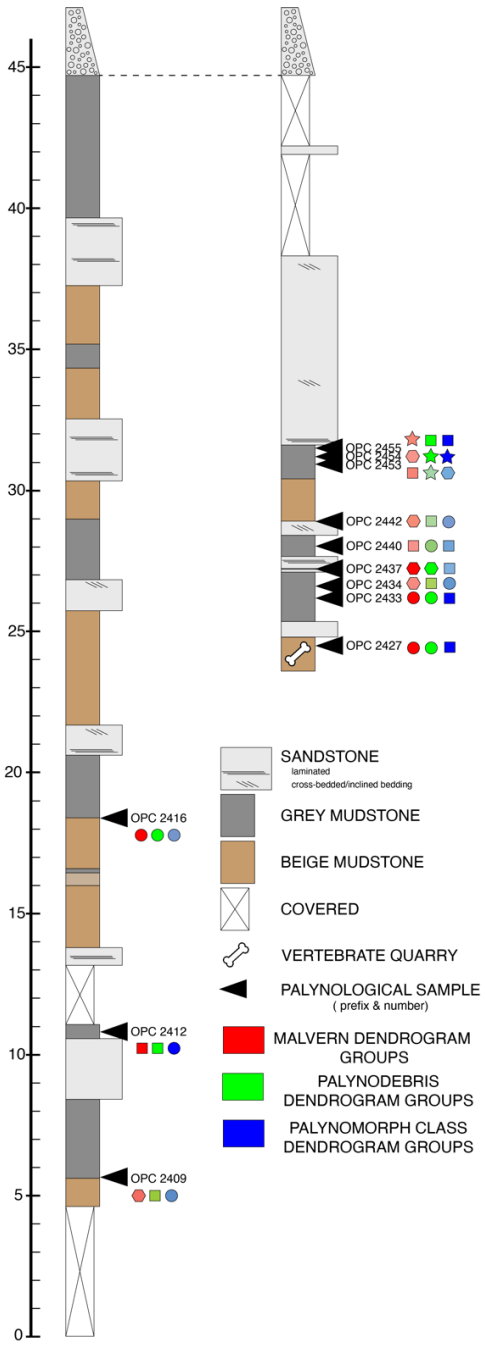

TABLES

Table 1. Comparison table of the features of the Moreno Hill Formation wood specimens to the fossil taxa *Cupressinoxylon manuelli* and *Taxodioxylon albertense,* and modern taxa*, Juniperus virginiana* and *Taiwania cryptomerioides.* KEY: – feature absent; --+ rare; -+ uncommon; + common, ++ very common; ?? data absent; ab abietinean orientation; ar araucarian orientation; sm smooth; nb notched border.

Wood Anatomy	OPC2462	OPC2464	OPC2465	OPC2469	*Cupressinoxylon manuelli*	*Taxodioxylon albertense*	*Juniperus virginiana*	*Taiwana cryptomerioides*
Growth ring boundaries	distinct	distinct	distinct	distinct	distinct	distinct	distinct	distinct
EW/LW Transition	gradual	gradual	gradual	gradual	gradual	abrupt	gradual	gradual
Tangential tracheid diameter[µm]	30(16-45)	35(13-55)	30(18-55)	31(15-60)	40(31-50)	?(16-24)	28(12-45)	35(16-55)
Tracheid pitting in radial walls								
uniseriate	++	++	++	++	++	++	++	++
biseriate	--+	--+	--+	--+	--+	-+	--+	-+
triseriate	-	-	-	-	-	-	-	-
Bordered pit arrangement	ab,ar	ab,ar	ab,ar	ab,ar	ab,ar	ab,ar	ab,ar	ab,ar
Bordered pit outline	sm,nb	sm,nb	sm,nb	sm,nb	sm,nb	sm	sm,nb	sm,nb
Diameter[µm]	21(14-27)	17.3(11-22)	17.2(14.5-21.5)	18.4(13.3-22.1)	15.4(13.5-19)	19.5(13.4-24.5)	16.8(11.3-20.2)	??
Tracheid pitting in tangential walls	--+	--+	--+	--+	-	-	--+	--+
Axial parenchyma	diffuse	diffuse	diffuse	diffuse	diffuse	diffusc/zonate	diffuse	diffuse
Transverse walls	smooth	smooth	smooth	smooth	smooth	smooth	smooth	smooth
Rays								
Height (cells)	18(1-78)	14(1-53)	15(2-52)	20(1-49)	12(1-42)	16(1-61)	15(2-20)	16(2-35)
Height [µm]	389(28-1504)	293(31-943)	292(43-946)	355(25-891)	277(22-617)	397(56-1599)	??	??
uniseriate	++	++	++	++	++	+	++	++
biseriate (partial)	-+	-+	-+	-+	-+	+	-	-+
biseriate	--+	--+	--+	--+	--+	+	-	--+
triseriate	-	-	-	-	-	+	-	-
ray tracheids	-+	-+	-+	-+	-	??	--+	-+
Cross-field pitting	cupressoid	cupressoid	cupressoid	cupressoid	cupressoid	taxodioid	cupressoid	cupressoid/taxodioid
pits per field	1-2	1-2	1-2	1-2	1-2	1-2	1-2	1-3
Helical thickening	-	-	-	-	-	-+	-	??

Table 2. IAWA softwood features used to compare MHF wood specimens to *J. virginiana.* Shared features are highlighted yellow.

40	Growth ring boundaries distinct
43	Gradual transition from earlywood to latewood
44	IT pitting (predominantly) uniseriate
46	IT pitting opposite
50	LT length short (less than 3000 µm)
53	Intercellular spaces throughout the wood
54?	LW LTs thin-walled (double wall thickness < radial lumen diameter)
55?	LW LTs thick-walled (double wall thickness > radial lumen diameter)
56	Torus present
58	Torus extensions
59	Pits with notched borders
60	Warty layer visible with light microscope
72	Axial parenchyma (AP) present
73	Diffuse axial parenchyma
74	Tangentially zonate axial parenchyma
78	Beaded or nodular AP transverse end walls
80	Ray tracheids absent or very rare
86	Distinctly pitted end walls of ray parenchyma cells
87	Smooth (unpitted) horizontal walls of ray parenchyma cells
89	Indentures
93	Cupressoid
98	1-3 pits per cross-field
99v	3-5 pits per cross-field
103	Average ray height medium (5 to 15 cells)
107	Rays exclusively uniseriate
19	North America, north of Mexico

PLATES

Plate I. Images of radial sections of Moreno Hill Formation specimens OPC2462-40600, OPC2464-40621, OPC2465-40645 and OPC2469-40654. Scale bar length and stage coordinates of image locations provided.

Figure 1. Cross-field pits of OPC2462. Scale bar 50µm. 146.9x14.0

Figure 2. Tracheid pitting behavior in OPC2462. White arrows point to zonate area of contiguity of bordered pits. Scale bar 100µm. 118.7x41.0

Figure 3. Spiral crushing near cross-field zones in OPC2462. Scale bar 50µm. 133.7x19.1

Figure 4. Notched bordered morphology in tracheid bordered pits in OPC2462. Scale bar 50µm. 1270x375

Figure 5. Cross-field pits of OPC2464. Scale bar 50µm. 121.9x33.7

Figure 6. Tracheid pitting behavior of OPC2464. Scale bar 100µm. 127.5x41.5

Figure 7. Spiral crushing near cross-fields in OPC2464. Scale bar 50µm. 134.1x41.5

Figure 8. Notched bordered tracheid pits in OPC2464. Scale bar 50µm. 124.5x30.5

Figure 9. Cross-fields of OPC2465. Scale bar 50µm. 108.8x43.2

Figure 10. Tracheid pit behavior of OPC2465 white arrows show contiguous bordered pits. Scale bar 100µm. 133.2x09.3

Figure 11. Spiral deformation proximal to cross-fields in OPC2465. Scale bar 50µm. 1320x320

Figure 12. Notched bordered tracheid pits in OPC2465. Scale bar 50µm. 152.5x28.0

Figure 13. Cross-fields in OPC2469. Scale bar 50µm. 145.0x22.7

Figure 14. Tracheid pitting habit in OPC2469, white arrows show contiguous bordered pits. Scale bar 100µm. 112.1x16.5

Figure 15. Spiral deformation proximal to cross-fields in OPC2469. Scale bar 50µm. 160.0x40.0

Figure 16. Tracheid pits with notched borders in OPC2469. Scale bar 50µm. 151.8x29.6

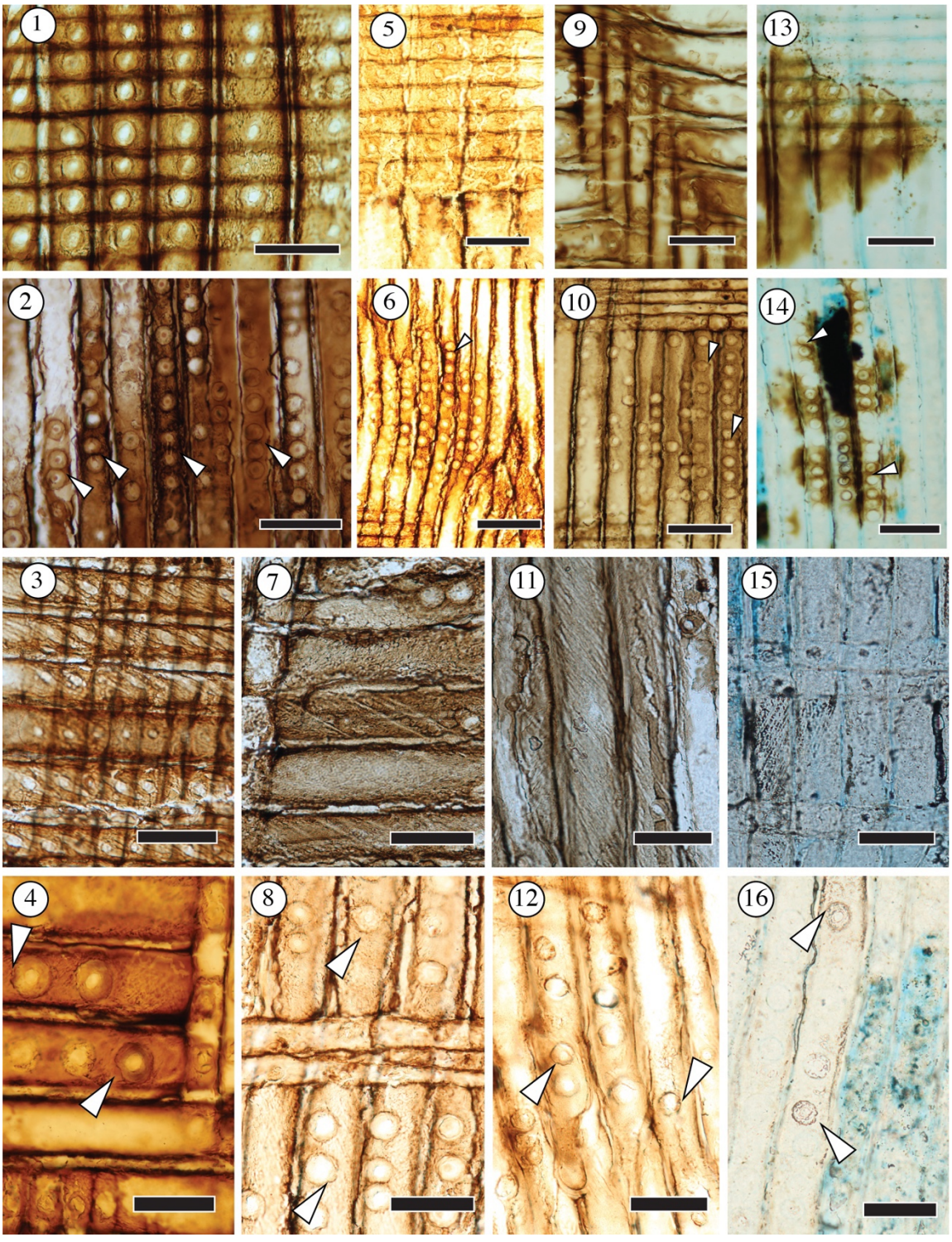
1
5
9
13
2
6
10
14
3
7
11
15
4
8
12
16

Plate II. Images of tangential sections of the Moreno Hill Formation specimens OPC2462-40598, OPC2464-40619, OPC2465-40643, and OPC2469-40652. Scale bar length and stage coordinates of image locations provided.

Figure 1. OPC2462 in tangential view illustrates the ray seriation habit. White arrow shows axial parenchyma with smooth end walls. Scale bar 500µm. 136.1x28.0

Figure 2. Bordered pits found on the tangential walls of the tracheids in OPC2462. Scale bar 50µm. 130.5x31.7

Figure 3. OPC2464 in tangential view. Shows the predominantly uniseriate ray habit. White arrows show axial parenchyma. Scale bar 500µm. 136.6x35.0

Figure 4. Tracheid pitting on the tangential walls of OPC2464. Scale bar 50µm. 138.3x10.0

Figure 5. OPC2465 in tangential view showing primarily uniseriate ray cells. White arrow points to axial parenchyma with smooth rounded end walls. Scale bar 500µm. 132.5x46.0

Figure 6. Tracheid pitting of tangential walls in OPC2465. Scale bar 50µm. 125.9x18.3

Figure 7. OPC2469 in tangential view show the difference in seriation habit between OPC2469 and the other samples. White arrows show axial parenchyma. Scale bar 500µm. 118.5x21.9

Figure 8. Tracheid pitting of tangential walls of OPC2469. Scale bar 50µm. 133.4x19.9

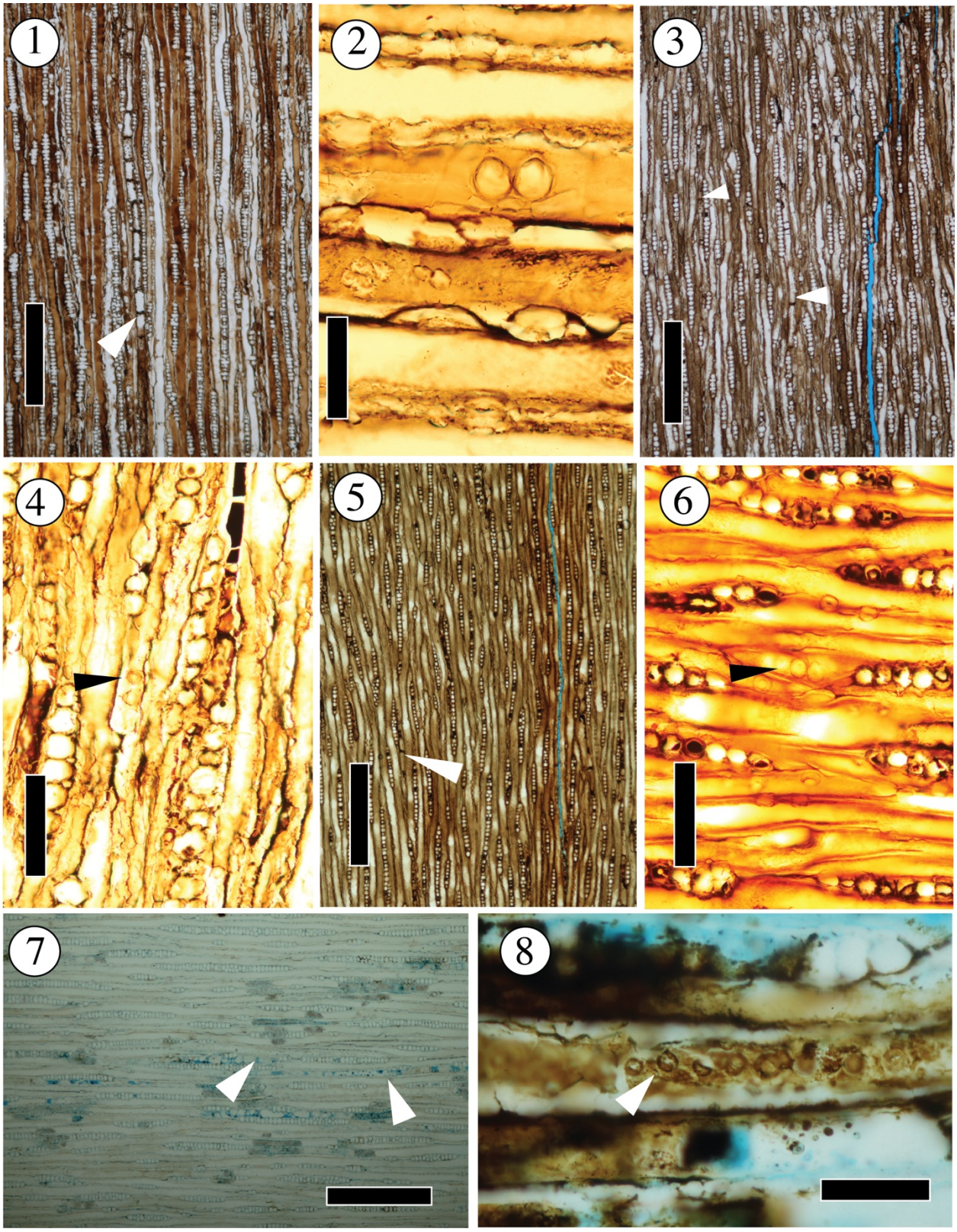
1
2
3
4
5
6
7
8

Plate III. Images of transverse section of Moreno Hill Formation specimens of OPC2462-40596, OPC2465-40641, and OPC2469-40650. Scale bar length and stage coordinates of image locations provided.

Figure 1. Lateral growth habit of OPC2462. White arrows denote diffuse axial parenchyma. Scale bar 1500µm. 129.7x20.5

Figure 2. Lateral growth habit of OPC2465 shows two seasonal rings. White arrows denote diffuse axial parenchyma. Scale bar 1500µm. 121.3x45.0

Figure 3. Lateral growth habit of OPC2469. What arrows denote diffuse axial parenchyma. Scale bar 1500µm. 118.5x19.8

Figure 4. Gradual earlywood to latewood transition in OPC2465. Growth ring boundary is distinct. Scale bar 500µm. 134.7x34.4

Figure 5. Gradual earlywood to latewood transition in OPC2469. Growth ring boundary is distinct. Scale bar 500µm. 143.3x34.5

Figure 6 Gradual earlywood to latewood transition in OPC2462. Destruction due to preservational stresses can be seen along the growth ring boundary. Scale bar 500µm. 131.9x42.5

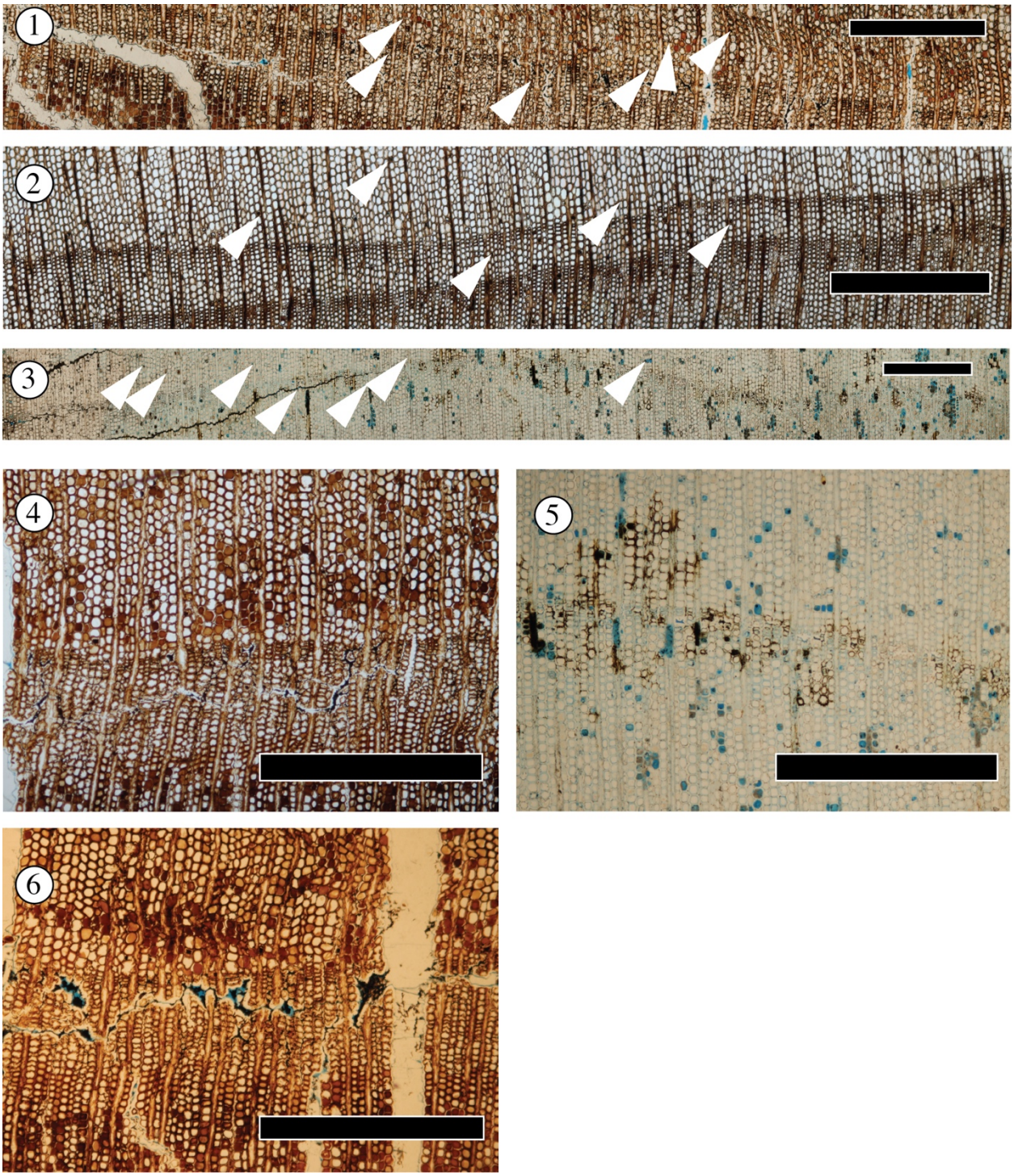
1
2
3
4
5
6

Plate IV. Images of wood sections of extant *Juniperus virginana* L..

Figure 1. Radial view showing cross fields with 1-2 cupressoid pits. Scale bar 50µm

Figure 2. Radial view showing tracheid pitting habit and bordered tracheid pits. Scale bar 50µm

Figure 3. Radial view with white arrows showing zonate contiguous tracheid pits. Scale bar 100µm.

Figure 4. Tangential view showing uniseriate ray cells. Scale bar 1000µm.

Figure 5. Tangential view showing tracheid pitting of the tangential walls. Scale bar 100µm

Figure 6. Tangential view showing axial parenchyma cells with smooth end walls. Scale bar 500µm.

Figure 7. Transverse view showing gradual earlywood to latewood transition and a distinct growth ring boundary. Scale bar 1500µm

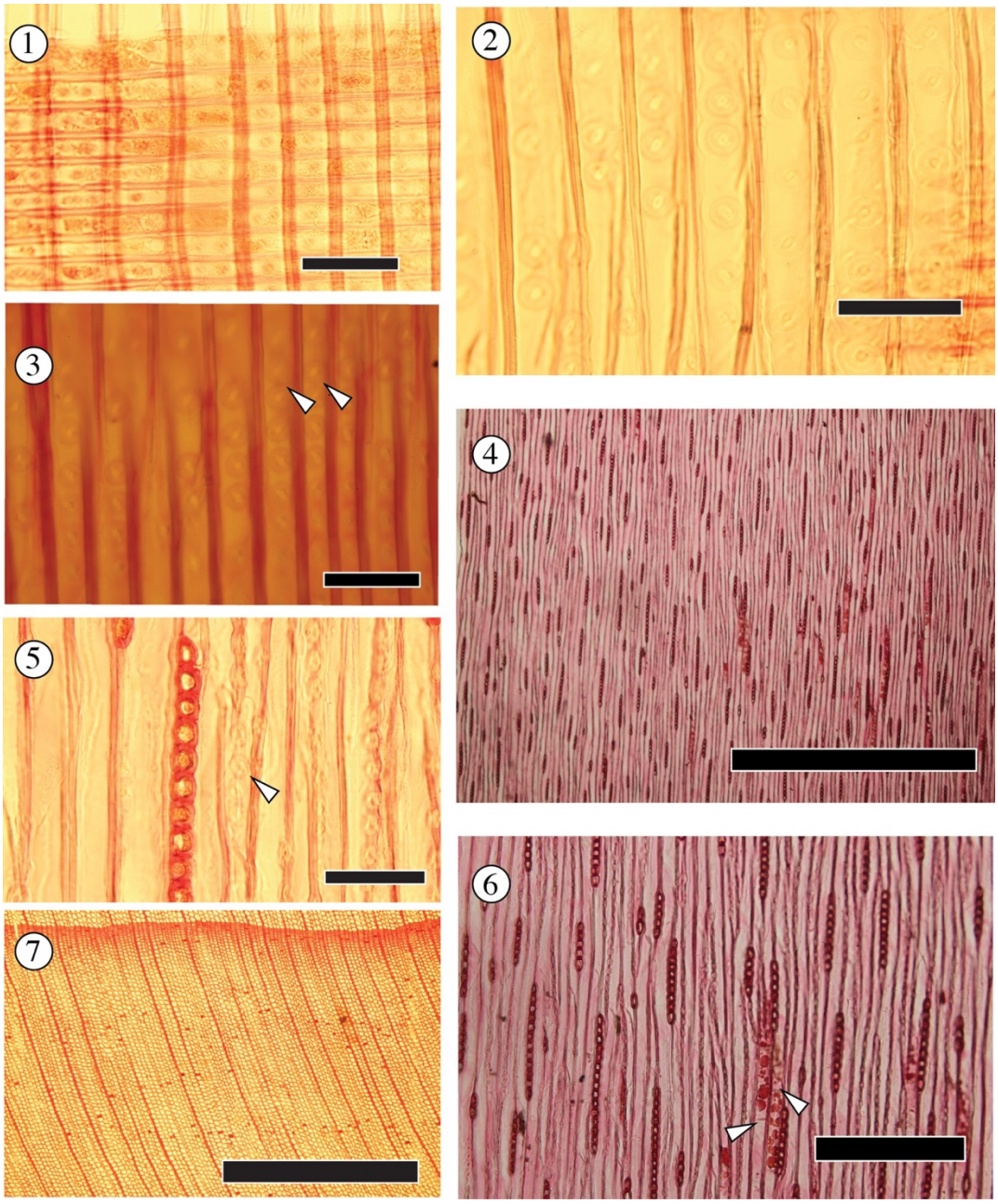
1
2
3
4
5
6
7

REFERENCES

Barber, C.A., 1898. *Cupressinoxylon vectense*; a fossil conifer from the Lower Greensand of Shanklin, in the Isle of Wight. Ann. Bot. os-12, 329–361. https://doi.org/10.1093/oxfordjournals.aob.a088698

Bamford, M.K. and Philippe, M., 2001. Jurassic–Early Cretaceous Gondwanan homoxylous woods: a nomenclatural revision of the genera with taxonomic notes. *Review of Palaeobotany and Palynology*, *113*(4), pp.287-297.

Batten, D.J., Stead, D.T., 2005. Palynofacies analysis and its stratigraphic application. Appl. Stratigr. 203–226.

Benton, M.J., Wilf, P., Sauquet, H., 2021. The Angiosperm Terrestrial Revolution and the origins of modern biodiversity. New Phytol. 233, 2017–2035. https://doi.org/10.1111/nph.17822

Boulter, M.C., 1994. An approach to a standard terminology for palynodebris, in: Traverse, A. (Ed.), Sedimentation of Organic Particles. Cambridge University Press, pp. 199–216. https://doi.org/10.1017/CBO9780511524875.012

Cilliers, C.D., Tucker, R.T., Crowley, J.L., Zanno, L.E., 2021. Age constraint for the Moreno Hill Formation (Zuni Basin) by CA-TIMS and LA-ICP-MS detrital zircon geochronology. PeerJ 9, e10948.

Combaz, A., 1964, Les palynofaciès: Revue de Micropaléontologie, vol. 7, p. 205–218.

Francis, J.E., Frakes, L.A., 1993. Cretaceous climates. Sedimentol. Rev. 1, 17–30.

Guzhikova, A.A., Guzhikov, A.Yu., Pervushov, E.M., Ryabov, I.P., Surinskiy, A.M., 2019. Existence of the reversal polarity zones in Turonian-Coniacian from the Lower Volga (Russia): new data, in: Nurgaliev, D., Shcherbakov, V., Kosterov, A., Spassov, S. (Eds.), Recent Advances in Rock Magnetism, Environmental Magnetism and Paleomagnetism, Springer Geophysics. Springer International Publishing, Cham, pp. 353–369. https://doi.org/10.1007/978-3-319-90437-5_25

Guzhikova, A.A., Pervushov, E. M., Pervushov, Evgeny M., Ryabov, I.P., Fomin, V.A., 2020. The reversal polarity zone in Turonian-Coniacian of the northern end of DonoMedvediza Dislocations. Изв. Сарат. ун-та. Нов. сер. Сер. Науки о Земле. 20, 262–277. https://doi.org/10.18500/1819-7663-2020-20-4-262-277

Haenggi, W.T., 2002. Tectonic history of the Chihuahua trough, Mexico and adjacent USA, Part II: Mesozoic and Cenozoic. Bol. Soc. Geológica Mex. 55, 38–94.

Herrera, F., Shi, G., Knopf, P., Leslie, A.B., Ichinnorov, N., Takahashi, M., Crane, P.R., Herendeen, P.S., 2017. Cupressaceae conifers from the Early Cretaceous of Mongolia. Int. J. Plant Sci. 178, 19–41.

Hoffman, G.K., 1994. Coal geology of the lower Moreno Hill Formation, Salt Lake Field, West Central New Mexico, in: New Mexico Geological Society Guidebook, 45th Field Conference, Mogollon Slope, West Central New Mexico and East-Central Arizona. pp. 283–290.

Hoffman, G.K., 2021. Influence of depositional environment on clay mineralogy in the coal-bearing lower Moreno Hill Formation, Salt Lake coal field, west-central New Mexico.

Kauffman, E.G., 1985. Cretaceous evolution of the Western Interior Basin of the United States.

Kelley, K.C., 1987 Palynologic investigation of the Moreno Hill Formation (Upper Cretaceous), West—central New Mexico. Unpublished M.S. Thesis. Michigan State University

Knowlton, F.H., 1888. Description of two species of fossil coniferous wood from Iowa and Montana. Proc. U. S. Natl. Mus. 5–8.

Kraus, M.J., 1999. Paleosols in clastic sedimentary rocks: their geologic applications. Earth-Sci. Rev. 47, 41–70.

Lawson, E.R., 1990. *Juniperus virginiana* L. eastern redcedar. Silv. N. Am. 1, 131–140.

Little, D.P., 2006. Evolution and circumscription of the true cypresses (Cupressaceae: *Cupressus*). Syst. Bot. 31, 461–480.

Lucas, S.G., Heckert, A.B. and Sullivan, R.M., 2000. Cretaceous dinosaurs in New Mexico. *Dinosaurs of New Mexico. New Mexico Museum of Natural History and Science. Bulletin*, *17*, pp.83-90.

Lutz, H.J., 1930. A new species of *Cupressinoxylon* (Goeppert) Gothan from the Jurassic of South Dakota. Bot. Gaz. Chic. Ill 90, 92–107. https://doi.org/10.1086/334086

Mack, G.H., 1992. Paleosols as an indicator of climatic change at the early-late Cretaceous boundary, southwestern New Mexico. J. Sediment. Res. 62, 483–494.

Malvern Analytical, 2015.A Basic Guide to Particle Characterization.Particle Characterization Guide. Malvern Instruments Worldwide.

McIver, E.E., 2001. Cretaceous *Widdringtonia* Endl.(Cupressaceae) from North America. Int. J. Plant Sci. 162, 937–961.

Page, C.N., 1990. Cupressaceae, in: Pteridophytes and Gymnosperms. Springer, pp. 302–316.

Petersen, M.R., Hill, R.W., 1985. Evapotranspiration of small conifers. J. Irrig. Drain. Eng.-Asce 111, 341–351. https://doi.org/10.1061/(asce)0733-9437(1985)111:4(341)

Philippe, M. and Bamford, M.K., 2008. A key to morphogenera used for Mesozoic conifer-like woods. *Review of Palaeobotany and Palynology*, *148*(2-4), pp.184-207.

Riddle, J., 2011. Growth-climate relationships of *Juniperus communis* and *Juniperus virginiana* at contrasting range margins. Unpublished M.S. Thesis. State University of New York College of Environmental Science and Forestry.

Ríos-Santos, C., Cevallos-Ferriz, S.R., Pujana, R.R., 2020. Cupressaceous woods in the upper Cretaceous Cabullona Group in Fronteras, Sonora, Mexico. J. South Am. Earth Sci. 104, 102756.

Singh, N., Singh, J., Gupta, A.K., Bräuning, A., Dimri, A.P., Ramanathan, Al., A. L. Ramanathan, Sharma, V., Tiwari, R.K., Chakraborty, J.S., Chauhan, P.K., Chauhan, P., Shukla, T., Singhal, M., Rawat, S., Agarwal, S., Raja, P., P. Raja, 2021. Climate-driven acceleration in forest evapotranspiration fuelling extreme rainfall events in the Himalaya. Environ. Res. Lett. 16, 084042. https://doi.org/10.1088/1748-9326/ac14ed

Sweeney, I.J., Chin, K., Hower, J.C., Budd, D.A., Wolfe, D.G., 2009. Fossil wood from the middle Cretaceous Moreno Hill Formation: Unique expressions of wood mineralization and implications for the processes of wood preservation. Int. J. Coal Geol. 79, 1–17.

Tyson, R.V., 1993. Palynofacies analysis. Appl. Micropalaeontology 153–191.

Vakhrameev, V.A., 1981. Pollen *Classopolis*: indicator of Jurassic and Cretaceous climates. J. Palaeosciences 28, 301–307. https://doi.org/10.54991/jop.1981.1417

Weller, A.F., 2004. The semi-automated classification of sedimentary organic matter and dinoflagellate cysts in palynological preparations. Doctoral Dissertation. University of Glanmorgan.

Weller, A.F., Harris, A.J., Ware, A., Ware, J.A., 2007. Two supervised neural networks for classification of sedimentary organic matter images from palynological preparations. Math. Geosci. 39, 657–671. https://doi.org/10.1007/s11004-007-9120-x

Wolfe, D.G., Kirkland, J.I., Lucas, S.G., 1998. *Zuniceratops christopheri* n. gen. & n. sp., a ceratopsian dinosaur from the Moreno Hill Formation (Cretaceous, Turonian) of west-central New Mexico. Low. Middle Cretac. Terr. Ecosyst. N. M. Mus. Nat. Hist. Sci. Bull. 14, 303–317.

Yonkee, W.A., Weil, A.B., 2015. Tectonic evolution of the Sevier and Laramide belts within the North American Cordillera orogenic system. Earth-Sci. Rev. 150, 531–593.